ON THE SETUP OF A SHORT LENS BETA SPECTROMETER

By

H.L. DE VRIES

A Thesis Submitted in Partial Fulfilment
of the Requirements for the Degree of
MASTER OF SCIENCE
in
NUCLEAR ENGINEERING

FACULTY OF SCIENCE
UNIVERSITY OF OTTAWA

TABLE OF CONTENTS

I. ABSTRACT

The spectrometer was originally designed and built by the AECL, Nuclear Physics Branch, in an experiment to determine the neutron lifetime (1). It was then acquired by the University of Ottawa in order to do experiments in the Nuclear Physics Lab, among which the determination of the exact shape of the continuous beta spectrum of P^{32}.

The present work describes the spectrometer and associated apparatus, the tests which are done after re-assembling and the final calibration with a Cs^{137} and a Tm^{170} source.

Conclusions are drawn as to the performance of the instrument and to the purposes for which it could be used.

II. GENERAL DESCRIPTION OF SPECTROMETERS

A. Introduction

In beta-ray spectroscopy use is made of magnetic and electric fields to deflect and focus the emitted particles in order to determine their energies and numbers. Instruments employing a magnetic field can be classified as (i) the flat type in which the particles are forced to describe a circular path and (ii) the lens type in which the particles describe helical paths. There are also spectrometers using an electrostatic field. These are employed for particles of very low energies only. K. Siegbahn gives detailed information about the various types in use (2).

B. Flat type spectrometers

(i) Permanent Magnet, 180° deflection, see Fig. 1.

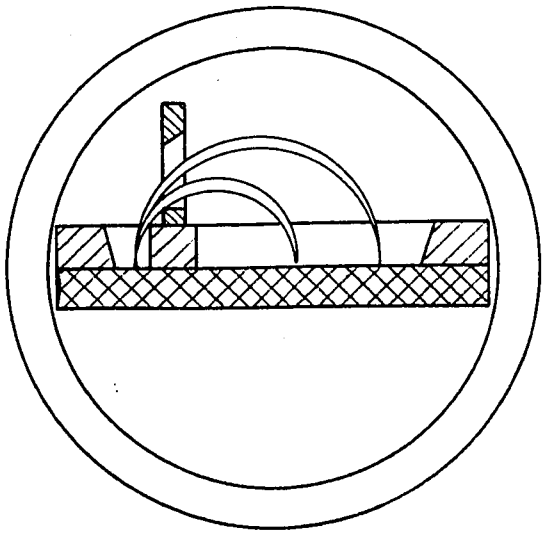

Fig. 1

The source is placed between pole pieces, i.e. in a homogeneous field so that the beta particle describes a circular path with a radius proportional to its momentum and in a direction determined by the sign of its charge. Hence, a photographic plate placed 180° from the source blackens there where particles are captured. One finds a non uniformly blackened area plus one or more lines. Spacings between the lines are a measure of the energy of the particles which are ejected in the process of internal conversion.

This type has the advantage of low cost, convenient calibration of the magnetic field to a high degree of accuracy from a conversion line of known momentum and the possibility to use photographic plates on which a large part of the spectrum can be registered. The transmission - the ratio of particles detected to particles emitted - is quite low, because only a narrow beam can be passed from the source in order to get reasonable resolution, and because the particles are focussed in one plane. Also, it is difficult to derive intensities of radiation from the degree of photographic blackening (3).

(ii) Variable field, 180° deflection.

When the field is varied the beta particles describe orbits of different radii. Hence one can focus particles of a certain energy on say, a counter. Thus both momentum and intensity can be measured.

Since focussing only occurs in one plane the transmission of such an instrument is relatively low.

(iii) Variable field, double focussing

Space focussing can be obtained by varying the field radially as:

$$H = H_0 . r.^{-\frac{1}{2}} \qquad (1)$$

An optimum condition for focussing in two planes is obtained when the particles are deflected over $\pi\sqrt{2}$ radians. A resolution of .01% is possible while the transmission is very much improved. The field, however, has to be more carefully shaped than given by (1), i.e. further terms containing powers of r are involved. This type employs sometimes iron pole pieces to shape the field. The iron, however, causes local distortions of the field due to inhomogneity of the material. The trend is to avoid the use of iron and to shape the field by means of an arrangement of coils.

C. Lens Spectrometer

(i) Principle

Electrons and positrons are focussed by magnetic fields in very much the same manner as light by optical lenses (4). This principle is applied to the lens spectrometer which may have either thin or thick lenses. This type has been thoroughly investigated because of its low cost and reasonable figure of merit.

The focussing action of a long solenoid creating a homogeneous field is treated in some detail, see Fig. 2. Consider a beta particle emitted from a thin source, i.e., not subjected to straggling. Its velocity can be resolved in a velocity parallel to the lines of the field: v_z and a velocity perpendicular to the lines of the field: v_r. Now the magnetic field acts on v_r only. Hence the particle is accelerated to describe a circular path, given by:

$$\frac{eHv_r}{c} = \frac{mv_r^2}{r} \qquad (2)$$

where:

H: strength of the field in gauss

r: radius of described circle

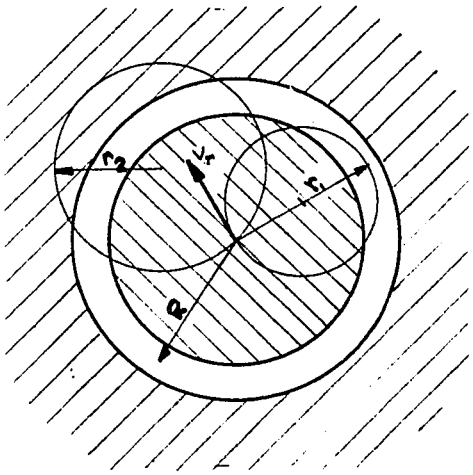

Fig. 2

m; the mass of the particle, which in beta-spectroscopy always has to be taken relativistically because of high velocities

e; unit of electro-static charge

c; velocity of light

The particle has also a forward component of motion, considering those of the isotropically emitted particles which reach the detector. The total motion can be thought of as being described along the surface of a right cylinder, i.e. helical. Now assume a baffle midway between source and counter having an annular slit. If the adjustment is such that all "cylinders" are tangent to the geometrical axis of the spectrometer, then those particles are detected which have $r = \frac{1}{2}(R + \Delta R)$, i.e. they are about 180° deflected at the place of the baffle and they return to the axis just there where the detector is located, assuming a point source and point detector.

From (2):

$$r = \frac{mv_r c}{eH} \qquad (3)$$

and from the requirement for detection:

$$r = \tfrac{1}{2}R$$

then:

$$v_r = \frac{ReH}{2mc} \tag{4}$$

The time of flight for both motions is equal:

$$t = \frac{2\pi r}{v_r} = \frac{l}{v_z} \tag{5}$$

Where

l; distance source-detector

Hence:

$$v_z = \frac{leH}{2\pi mc} \tag{6}$$

The momentum of the particle is given by:

$$p = mv \tag{7}$$

Then:

$$\begin{aligned} p^2 &= m^2v^2 \\ &= m^2(v_r^2 + v_z^2) \\ &= \left(\frac{ReH}{2c}\right)^2 + \left(\frac{leH}{2\pi c}\right)^2 \\ &= \frac{e^2H^2}{4c^2}\left(R^2 + \frac{l^2}{\pi^2}\right) \end{aligned} \tag{7a}$$

From the last equation fdlows that the momentum of the particle is proportional to the field.

From: $p = mv$

$E = mc^2$

$T = E - m_o c^2$,

it can be shown that:

$$p^2c^2 = T^2 + 2Tm_oc^2,$$

Where T is the kinetic energy of the particle.

Hence:

$$T^2 + 2Tm_oc^2 = \frac{e^2H^2}{4}\left(R^2 + \frac{l^2}{\pi^2}\right)$$

i.e.:

$$\frac{T}{m_oc^2}\left(\frac{T}{m_oc^2} + 2\right) = \frac{e^2H^2}{4\pi^2}\left(\pi^2R^2 + l^2\right)$$

and:

$$H = \frac{2\pi m_oc^2}{e\sqrt{\pi^2R^2 + l^2}}\sqrt{\frac{T}{m_oc^2}\left(\frac{T}{m_oc^2} + 2\right)} \qquad (8)$$

$$= 122.2\sqrt{\frac{T}{m_oc^2}\left(\frac{T}{m_oc^2} + 2\right)} \text{ GAUSS}$$

for our set up.

(8) also relates the main dimensions of the spectrometer to the energy of the particles. It can be seen that the factors R and l appear in the same order of magnitude.

The case for a curved magnetic field is quite difficult to treat mathematically since r varies with the shape of the

field. The particle now describes half a lemniscate instead of a circle if one projects its path on a plane perpendicular to the axis. The assumptions made in the calculations have to be checked experimentally.

(ii) Thick lens spectrometer, See Fig. 4

The field strength can be measured to one part in 10^4. Hence, line spacings can be determined accurately.

This type, however, suffers from spherical aberration in case of high transmission. In case of high resolution the source needs to be very small and the adjustments are very critical, hence the luminosity - transmission times source area - is very small. It is difficult to shield the detector, especially a photomultiplier, from the magnetic field. In the latter case one has often to resort to a long light pipe. The long solenoid spectrometer is otherwise easy to design.

(iii) The thin lens spectrometer

This type is widely used because of the advantages of variable magnification, convenient accessibility of source and counter, large solid angles, rather small size and small expenditure of capital (5).

The principle of the focussing action of a short solenoid depends upon chromatic aberration just as in the case of a long solenoid, i.e., dispersion in the strongly curved

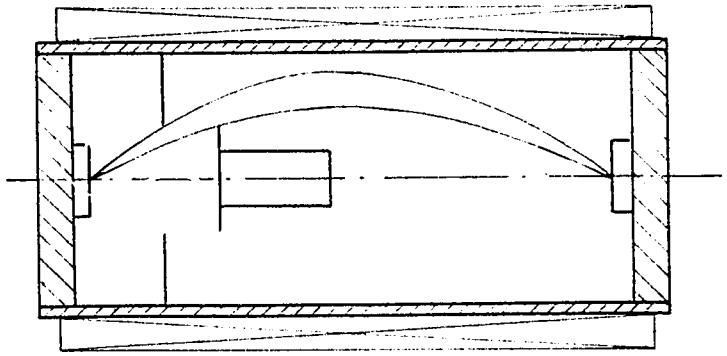

Fig. 4

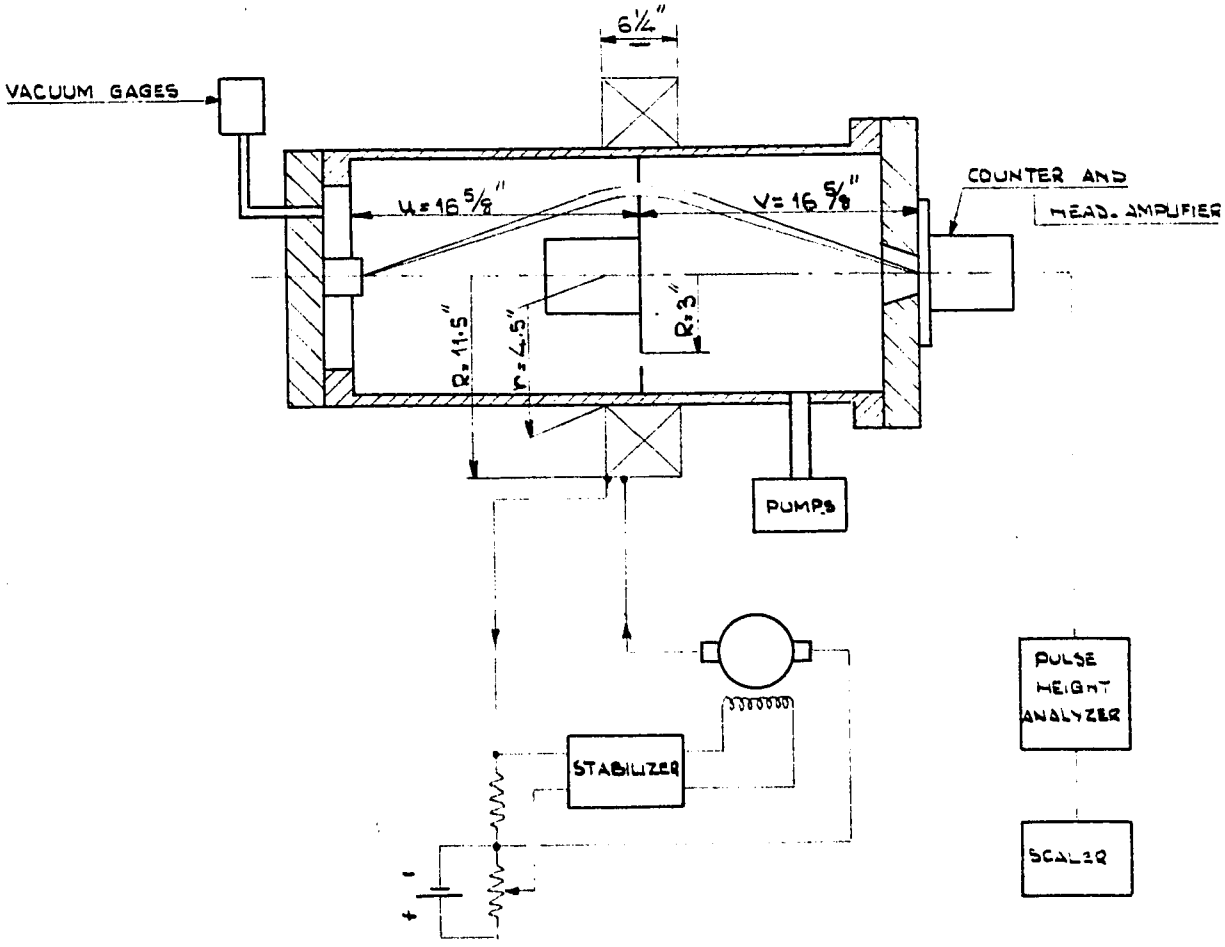
6¼"
VACUUM GAGES
U=16 5/8"
V=16 5/8"
COUNTER AND
HEAD. AMPLIFIER
R=11.5"
r=4.5"
R=3"
PUMPS
STABILIZER
PULSE HEIGHT ANALYZER
SCALER
-
+

Fig. 5

magnetic field will occur causing electrons of various wavelengths to focus on the image at different places. In fact, baffles are provided to capture the particles which do not fall on the detector window, Fig. 5.

The focal length is given by:

$$\frac{1}{f} = \frac{1}{u} + \frac{1}{v} \tag{9}$$

and magnetically by the approximation:

$$f = \frac{2a}{\pi k^2} \tag{10}$$

where:

a; width of the field distribution curve at half height,

$$k; \quad \frac{H_o \, a}{2H\rho} \tag{11}$$

H_o: the field strength at the centre of the coil

$H\rho$: the momentum of the electron to be focussed

The image is subjected to rotation:

$$\theta = \frac{\pi k}{\sqrt{k^2 + 1}} \tag{12}$$

Positrons and electrons exhibit opposite senses of rotation and can be separated by the use of a so called paddle-wheel. It has vanes shaped such that particles of one kind are allowed to spiral through the grooves while particles of the other kind, spiralling in the opposite sense, are stopped by the vanes.

A thin lens will always cause spherical aberration, i.e., partial focussing in front of the image plane. This is due to the fact that the outer part of the lens focusses with shorter focal lengths than the middle part because of the difference in angles of incidence. Its influence on the theoretical resolving power can be found both mathematically and, much simpler, by experiment.

The resolving power, or shortly resolution, is defined as the width of the curve at either the base, R_o, or at half height, R. Geometrically, it can be found as follows.

Suppose the path of the spiralling particle is straightened out and projected in a flat plane as shown in fig. 5a.

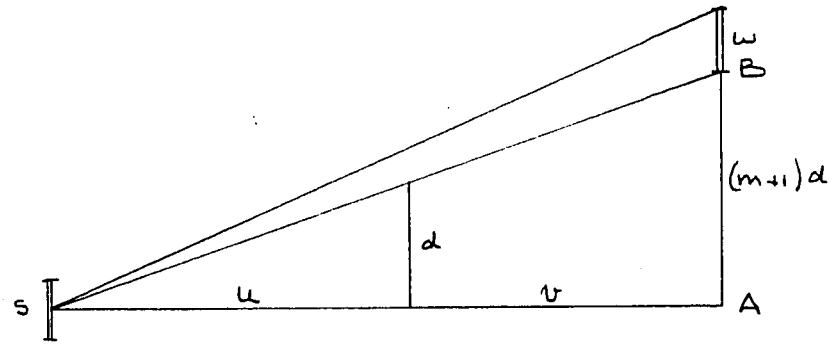

FIG. 5a

Where: S; the diameter of the source window,

w; the diameter of the counter window,

d; the radius of the slit in the baffle,

$u + v = f$, the focal length,

and $m = \frac{v}{u}$, the magnification.

Suppose the field is kept constant, then the momentum of the particle is approximately proportional to the radius of the slit in the baffle, as given by equation (7a).

Hence:

$$p \propto d$$

$$\propto d \frac{u + v}{v} = d(m+1)$$ at the location of the counter window.

The side of the counter window W allows a spread $\Delta p'$ in the momentum, which is approximately proportional to the length W, if one considers a point source only. Similarly, a finite side S of the source window causes a spread $\Delta p''$. This spread, however, is measured at the counter side instead of the source side and has therefore to be multiplied by the magnification:

$$\Delta p'' \propto mS$$

Hence:

$$R_o = \frac{\Delta p}{p} \simeq \frac{W + mS}{(m+1)d} \qquad (13)$$

If $u = v$, then the resolution at half height is:

$$R = \frac{R_o}{2} \simeq \frac{W + S}{2d} \qquad (14)$$

The transmission is approximately given by:

$$T = \frac{d \Delta d}{2u^2} \qquad (15)$$

where Δd = slit width in centre baffle.

Spherical aberration decreases the theoretical values considerably as can be seen from Chapter V. Careful design of the baffle system, however, will eliminate most of the spherical aberration (6).

III DESCRIPTION OF THE APPARATUS INSTALLED

A. Introduction

The general idea of our set up is given in Fig. 5. The source is mounted in s. The beta rays are focussed on an anthracene crystal in c, causing light flashes. These flashes are converted into electric pulses by the photo-multiplier in the head-amplifier. The pulses are fed to a single channel pulse height analyzer where they are discriminated by means of a variable lower bias setting, and if desired, an upper bias setting. A scale of 64 counts the output of the P.H.A.

The magnet current causes a linearly varying voltage drop over the 0.5 ohm resistor. This voltage is compared in the stabilizer with a reference voltage, set by a helipot control. The stabilizer output current generates the field in the generator. The magnitude of the magnet current is thus stabilized for any setting of the helipot control.

The vacuum is maintained by a mechanical pump plus a three stage diffusion pump. It is measured by pirani gages and an ion gage.

B. Vacuum chamber and vacuum system

The chamber consists of an aluminum tank, 7½" inner dia and 33 1/16" long. It is closed off on either side by flanges. The flange on the source side is of brass and supports

the vacuum gages which are mounted on two copper elbows in order to prevent light from leaking into the chamber. The source, consisting of a radio active deposit about 2mm in dia on a thin aluminum foil is mounted on an elevation on the flange, about 1½" high. This distance is sufficient to reduce back scatter to an insignificant level. The position of the active deposit is reproducible with an error of less than ½ mm.

The flange on the counter side is made of aluminum and supports the fish-eye holder and the phototube holder. Both source and detector end are provided with rubber gaskets which are placed in grooves. Although rubber gaskets may not be theoretically as good as a welded structure, they are essential if the system is to be demountable and are in general use. It is possible to obtain a vacuum of better than 10^{-6} mmHg with such gaskets if a cold trap filled with liquid N_2 is used. Such a vacuum is not necessary in a spectrometer of such length as discussed in the accompanying thesis of Y. Motoda. However, it happened that a vacuum of .1 micron of Hg could easily be maintained. Nevertheless, it appeared that the flange supporting the counter had a small light leak. This leak caused the counting rate at low bias setting to jump from 65 to 110 c/m. (It has to be noted that the bias setting of

the discriminator in this case was different from the setting for the background count as mentioned on page 18). The leak was remedied by covering the counter end with a black cloth.

The baffle system consists of a ring which is closely fitted to the chamber and a central disc leaving an annular slit of ¼". Gamma rays are attenuated by a lead stopper of about 4" long.

We were fortunate to have chamber and attachments, but for one flange, made of aluminum because it does not scatter beta particles as much as brass does (5). The background count was about 27 c/m if a 5 microcurrie Tm^{170} source was placed in the chamber. It should be possible to reduce the background by internal shielding against scattered particles (6).

The vacuum is maintained by a three stage, watercooled diffusion pump in conjunction with a mechanical pump. It is measured by a pair of Pirani gages - one tube with a reference vacuum and one connected to the chamber - and by an ion gage, which is switched on when the vacuum is 7 microns or better. The best vacuum obtained so far is .02 micron.

C. Magnet

A coil containing about 3600 turns surrounds the centre of the chamber. The CALCULATED field distribution for our coil is given in Fig. 6. It is mounted on a carrier which rolls on a pair of tracks. Furthermore, the coil can be elevated, shifted and swinged in various planes. Precise alignment of vacuum chamber with the magnet field proved to be a difficult and tedious task. It might be desirable to check the location and shape of the image by exposing a photographic

$$H = \frac{.2\pi IN}{r} \sin^3 \beta$$

Where β is the angle between the axis and a line from a point on the axis to be middle of the coil turns.

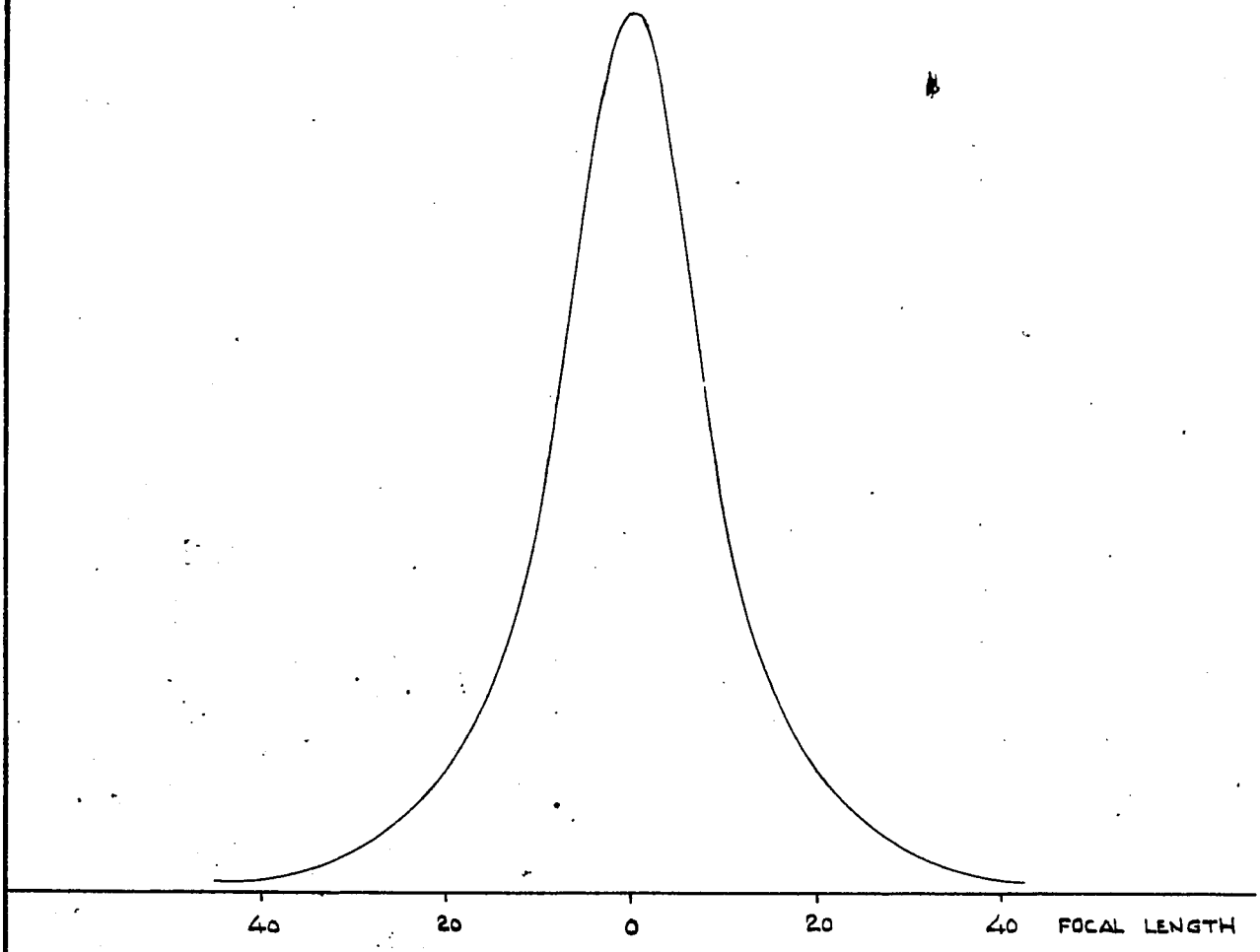

Fig. 6

plate in front of the phosphor to the focussed beam of beta particles. The vacuum chamber and coil tracks are rigidly mounted on a wooden table.

D. Degaussing coils

From the table is also supported a set of Helmholtz degaussing coils. These coils create a magnetic field which eliminates the vertical component of the earth magnetic field. They are described in extenso in the accompanying thesis of Y. Motoda (7). An auto storage battery furnishes the current for the degaussing coils.

The axis of the chamber is lined up with the earth magnetic field in order to prevent deflections of particles of the lower energies.

E. Generator, Electromagnet and Stabilizer

The wiring diagram is given in Appendix I. On the generator chassis are mounted a 3 phase, 550V motor, a D.C. generator and an exciter. A $\frac{1}{2}$ Ohm resistor is connected in series with generator and magnet in order to provide a voltage proportional to the magnitude of the magnet current.

The exciter, generating 60V, provides the source of current for the generator field. The magnitude of this current is controlled by a bank of 16 6AS7 tubes, which can be regarded as a variable resistor. This bank of tubes in turn is controlled by the stabilizer circuit as described

below.

The central element of the stabilizer is a 400 cycle chopper. It conducts alternatively the voltage over the ½ Ohm resistor and a reference voltage to a four stage amplifier. The reference voltage is obtained from dry cells, by means of a helipot. Its magnitude can thus accurately be reproduced.

A 6AC7 tube generates 400 cycles by means of a three stage capacitance coupled phase shift network, providing a 180° degree shift between plate and control grid. The plate of the oscillator is coupled to a potmeter by means of a capacitor. The bias on the amplifier stage is adjusted to drive the chopper with 6V. This value is not critical. The oscillator as well as the other stages in the stabilizer chassis are built in shielding boxes and heavily decoupled in order to prevent the occurrence of oscillations of the whole system.

Now the chopper feeds an alternating step function into the four stage amplifier. The control grids of the second, third and fourth amplifier contain an R-C network having a time constant of 1/400 sec in order to suppress harmonics and to round the step function off to a shape suitable for feeding the phase sensitive detector.

This detector is driven by an A-C voltage of 400 cycles whose amplitude is indicated by the voltmeter across transformer T3 and whose phase is controlled by the phasing

network of 100K Ohms variable resistor plus .05μF capacitor over the first 6SN7 triode. The phase has to be matched with the shifted phase of the output pulse of the amplifier. Every time both diodes are conducting, a pulse from T1 is superimposed on the current through the diodes causing one side to carry more current than the other. Hence the voltage drops over the 50K Ohm resistors become unequal and the grid of the cathode follower is biassed by their difference, while the galvanometer indicates an out-of-balance. The circuit is zeroed by a 7.5K Ohm potentiometer. The voltage drop over the 0.5 Ohm resistor in the magnet circuit is equal to the reference voltage if the galvanometer is zeored, i.e., a steady bias is supplied to the 6AS7 tubes instead of correcting pulses superimposed upon a non correct bias level. It is therefore imperative to adjust the 7.5K Ohm potentiometer to give zero current through the galvanometer in order to obtain an exact relation between magnet current and helipot settings. The plate of the output stage of the 6SH7 is coupled to ground through a 100K Ohm resistor and a mA meter. The voltage drop over this resistor provides the bias on the grids of the 6AS7 tubes and is indicated by the meter.

The plate current of the 6AS7 tubes passes through the field of the generator. The maximum value in the present set up is about 4 Amps, resulting in a magnet current of about 13 Amps. These values can be increased by using an

additional voltage source in series with the exciter. The experiments to be done, however, do not require large fields. Hence, the modification is omitted.

It is necessary to use feed back in order to prevent the system from oscillating. Two differentiating circuits are employed. First, a $2\mu F$ capacitor is connected across the magnet. It feeds a voltage proportional to the rate of change of current through the magnet into the chopper, i.e., some reliance is placed on the fact that the voltage across the coil is proportional to the rate of change of current through it. Another network is connected between the plates of the 6AS7 tubes and the control grid of the second 6SH7 triode correcting the bias on the 6AS7 tubes.

The power supply is of conventional design. One of the two phases of the secondary winding is used for a negative H.T. supply as well as for full wave rectification.

In addition to the circuits described, safeguards are incorporated against sudden breakdown and overheating.

There is a considerable amount of energy stored in the field of the magnet, once it is built up. This energy is converted into a high potential should the magnet current drop out suddenly. Therefore, a Tungar £as filled diode is employed providing an inertialess short as soon as the reverse potential exceeds 25V. The other safeguard consists of a trip circuit activated if the resistance of the magnet should increase above a certain value due to heating up. This could occur when the cooling water is turned off while the magnet carries a heavy current. As can be seen from the circuit diagram, the magnet is a branch of a Wheatstone Bridge. Another branch can be adjusted to match the resistance of the section of the magnet in use. A Weston Sensitrol galvanometer controls a relay in the power line to the motor.

F. Phosphor and photomultiplier

The wiring of the photomultiplier and cathode follower is to best suit the particular set up. Namely by taking the output pulse of the photomultiplier from the last dynode one collects positive pulses. The cathode follower provides a high impedance to the output of the photomultiplier. On the other hand, its cathode circuit possesses a low impedance. Hence, it is eminently suited to drive a coaxial cable with positive pulses.

The photomultiplier is an RCA 1P21 tube having a suitable signal to noise ratio by operation on 850V. The tube is placed in a mild steel holder in order to shield it from the magnetic field.

The beta particles are focussed on an anthracene phosphor of about 5 mm dia and about 2 mm thickness. It attenuates the incident particles such that about 80% are stopped in the phosphor thereby giving up all their energy. The remaining 20% leave the phosphor with very much reduced energies. These values are calculated from the end point energies of the continuous spectrum of Cs^{137}(7). The phosphor is embedded in a lucite light pipe, called fish-eye, which transmits the light flashes to the photo cathode. The phosphor end of the fish-eye is covered by an aluminum foil - 225 microgram/cm^2 - which reflects outgoing light back into the light pipe. The foil stops about 4% of the 22.7 KeV K peak electrons (8,9) of Tm^{170} while the rest is let through with reduced energies causing a shift of especially the K peak towards the lower end of the momentum scale and also an additional spread in the registered momenta.

G. Single channel pulse height analyzer

(i) Principle

This analyzer, of AECL design, consists principally of a phase inverter followed by a three stage amplifier, a lower and an upper channel discriminator and an anticoincidence mixer from which the standard output pulse is obtained, see Appendix II.

(ii) Operation of circuit elements

The input pulse is attenuated to the desired voltage by means of a chain of resistors and fed into a phase inverter. The sign of the pulse is changed by using the

inverter as a straight amplifier. In the other setting it functions as a cathode follower. The design calls for negative pulses at the input of the amplifier.

The amplifier consists of two sharp cut off pentodes followed by a beam power tube all coupled by simple RC networks. Overall gain for undistorted output is about 750. The positive output pulse is fed to the first stage of both channels: the cathode followers V5 and V18 and to another cathode follower, V22. The latter has an output jack at the rear of the chassis enabling one to study the shape of the pulses on an oscilloscope as they come from the photomultiplier.

The lower channel only will be described here since both channels are identical.

The bias of tube V5 is controlled by a 100K Ohm helipot, connected between ground and a regulated 75V supply, being in fact 72V. Adjusting the helipot from 0 to 1000 on the dial results in voltages on the control grid of V5 of +70V to +47V with the cathode following closely. The voltage of the cathode of the crystal diode is maintained at 75V while the cathode of V6 varies slightly with the bias on V5. The addition of V6 in series with the crystal diode is necessary in order to prevent the occurrence of back current since the crystal diodes do not cut off completely in the "forbidden" direction. See figure 7.

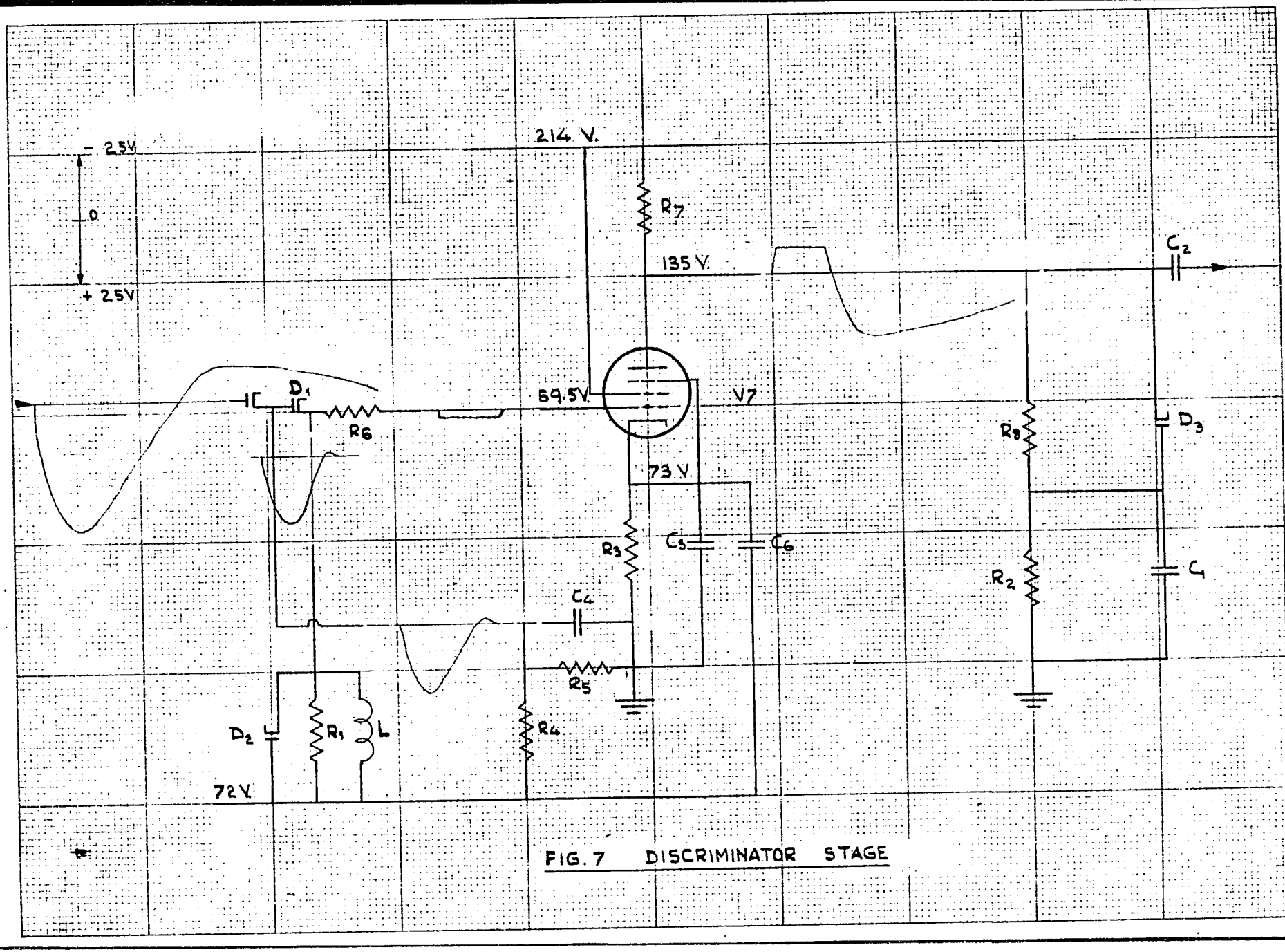

FIG. 7 DISCRIMINATOR STAGE

Pulse and regulated anode voltage have to add up to over and above 72V in order to cause D1 to conduct. The cathode of D1 is kept at a voltage of 72V because of the self inductance L which has a low DC resistance. Oscillations in the L-R network are prevented by diode D2 shorting a reversed potential to the 75V supply. The amplifier V7 is thus driven by a pulse caused by the trigger action in the discriminator.

The plate of the diode D3 is kept at about 10 volts below its cathode. Hence D3 limits the amplitude of the negative pulse in the plate line to about 10 volts, the excess being absorbed by capacitor C1. The positive pulse is blocked by the diode D1 of Fig. 8. The flip-flop stage is thus driven by a very well defined, negative pulse.

The tubes V8 and V9 are components of a modified Schmitt trigger circuit, also known as a voltage discriminator (10). Figure 8 shows the circuit with steady state voltages, i.e., when no signal of negative sign is applied to the cathode of D1. The bias on the control grid of V8 is then 1 volt. Hence, the tube is conducting causing a bias of 11 V on V9 which is cut off.

Now suppose a small negative signal is applied to the cathode of D1. It begins to conduct and the grid of V8 will be lowered in potential. The plate current of V8

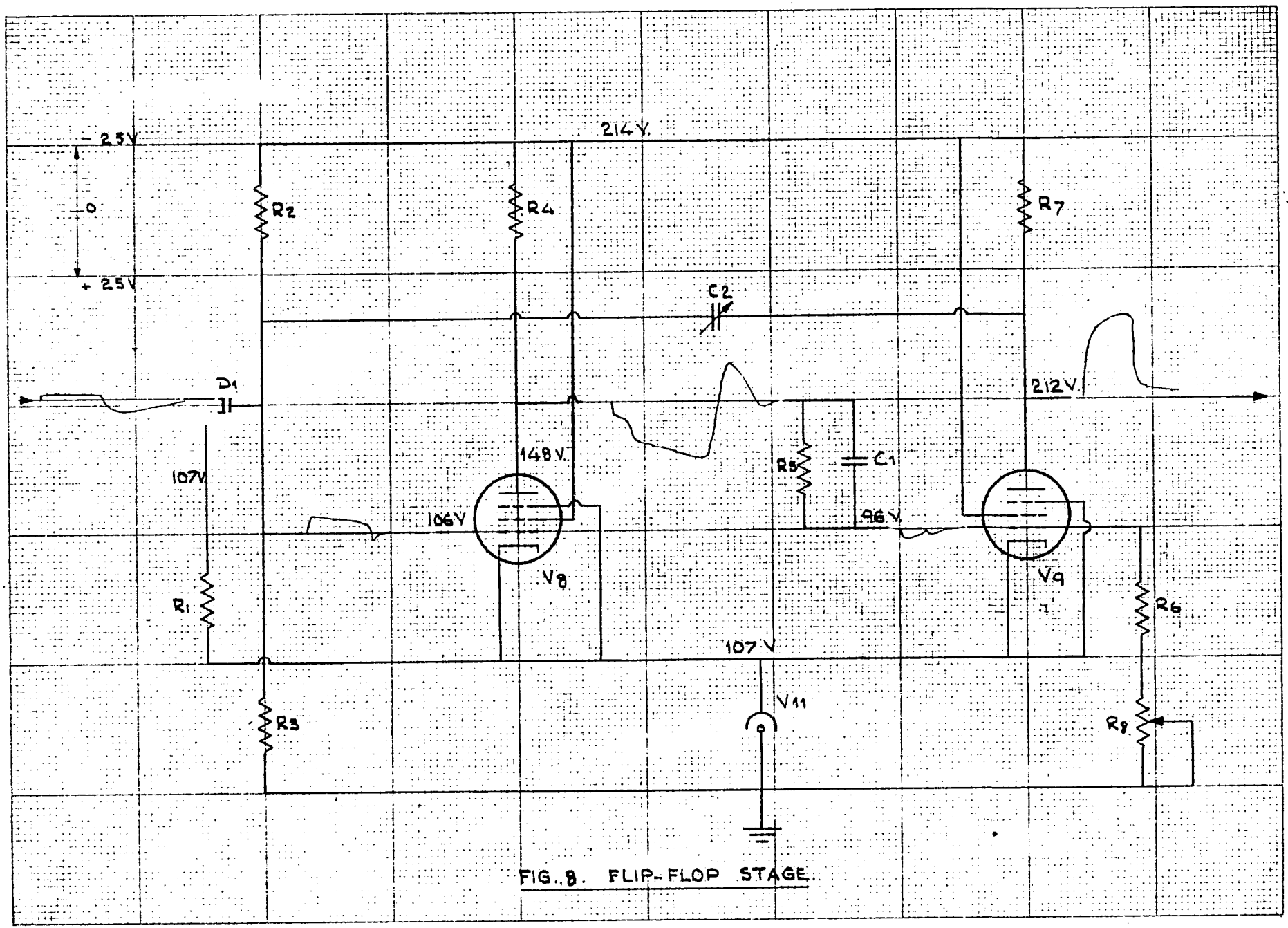

FIG. 8. FLIP-FLOP STAGE.

decreases and also the bias of V9 since the cathodes of V8 and V9 are supplied with a constant voltage from the regulator V11. The rising input pulse is amplified by V8 until V9 begins to conduct, producing a negative pulse on its anode. This pulse is fed back to the grid of V8 through C2 and adds in increasing the bias. Consequently, the pulse on the plate of V9 grows rapidly. V8 will be cut off and the circuit will attain a steady state.

The described process takes place almost at once since V9 can be biassed so as to be not completely cut off. The original Schmitt circuit differs in that a series of oscillations occurs during the transition of one steady state to another.

The time constant of the recovery of the grid of V8 is determined by C2 and R3 in parallel with R2 combined with the impedance of grid of V8 to plate of V9. The setting of C2 determines the time constant of this network, i.e., the time elapsing from the point where the negative pulse on the plate of V9 rises until the time the network swings back. C2 is to be adjusted for 1 microsecond. Now the initial negative pulse on the grid of V8 has died out in the meantime and the bias on V8 is restored to approximately 1 Volt. Therefore, by the time the network tends to swing back it is completely free to do so. Hence the grid potential

of V8 increases as a stepfunction and consequently V8 starts conducting thereby immediately reducing the plate current of V9 to a small value. The circuit is again in a steady state, the one we started from during our considerations.

Now the large negative pulse is put through a .25 μsec delay line, attenuated, and has to be compared with pulses from the upper channel in the anti-coincidence stages; see figure 9.

When no signals are applied, the first triode is conducting and the second is cut off. A negative pulse on the grid of the first triode lowers the cathode potential., the triode being connected as a cathode follower. This decreases the bias on the second triode and a pulse appears in the channel output. The simultaneous arrival of pulses from both channels, however, makes that the relative potential difference between cathode and grid of the second triode does not change appreciably so that the tube remains cut off and no pulse is delivered.

Diode D1 passes current in the network R3, R2, R8 which can be adjusted to give a proper bias on the second triode with respect to both pulses. Diode D2 serves to feed in the pulse from the upper channel which has a rather long decay time due to the high value of the leak resistor. Also, this pulse will lagg in phase relative to the pulse of the

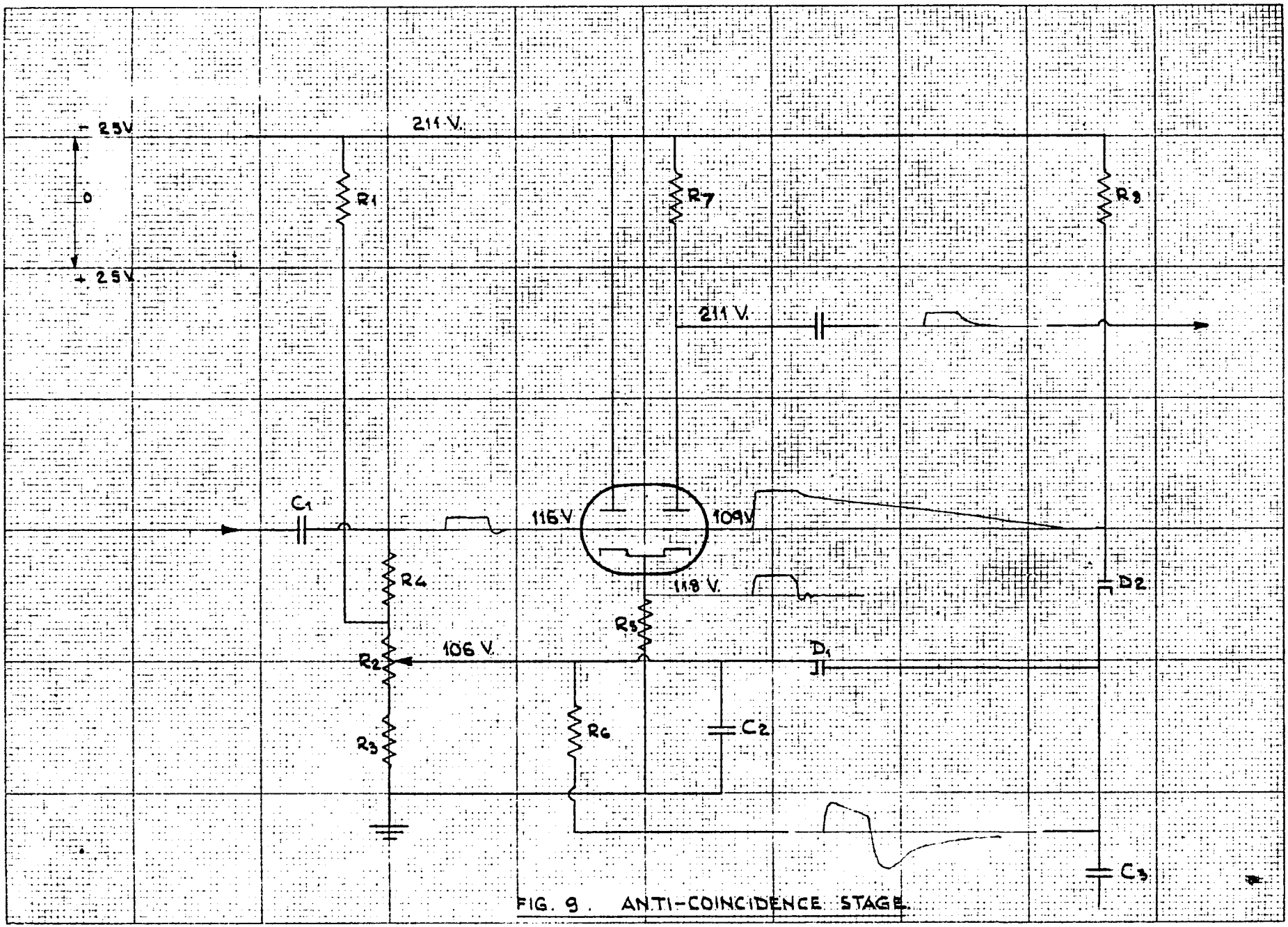

FIG. 9. ANTI-COINCIDENCE STAGE.

lower channel because on an incoming pulse of finite rise time the lower discriminator will always fire before the upper. It is essential that the pulse from the lower discriminator should arrive at the anti-coincidence circuit simultaneously or later to prevent feed through of the initial past of the pulse from the lower discriminator.

(iii) Summary.

The pulse height analyzer discriminates between pulses of different amplitudes by feeding them into two channels. The lower channel passes all pulses exceeding a preset bias voltage and stops the rest as does the upper channel but at a higher voltage. The output of both channels is combined in the anti-coincidence stage which fires only when a pulse is passed through the lower channel but falls short of the level of the upper channel. Hence it is possible to resolve a spectrum in counts per momentum interval: the difference between the bias levels, - at corresponding moments : the average bias levels.

(iv) Additional features.

(1) An adjustable window width obtained from dry cells. The cell voltage is superimposed upon the bias of the lower channel and then used to bias the upper channel. This enables one to scan a spectrum with a constant window.

(2) A triple coincidence circuit, which is not described here since it is not used yet.

(3) It is also possible to make use of a scan unit controlling the bias of the lower channel.

H. Pulse Generator

The basic idea of the pulse generator is to give pulses whose relative amplitude is accurately known. It is used for adjustment of the pulse height analyzer and for calibration of levels of discrimination.

The output voltage of the well regulated power supply is attenuated in two stages, see Fig. 10. They consist of helipots, while an extra 1 ÷ 10 attenuator can be switched in. A Western Electric Mercury Relay is employed. It charges a .005 mF capacitor from the power supply and discharges it through an RC output network at the recurrence frequency of 60 c/s.

J. Scale of 64

The scale of 64 is an Atomic Instrument Model 101A. Its operation is quite simple and straight forward and will be briefly described.

The input is connected to a Pulse Amplitude Discriminator consisting of two tubes which comprise a Schmitt trigger circuit. The operation of this circuit is described under the Pulse Height Analyzer. Discrimination is obtained by setting the bias level of the first tube a

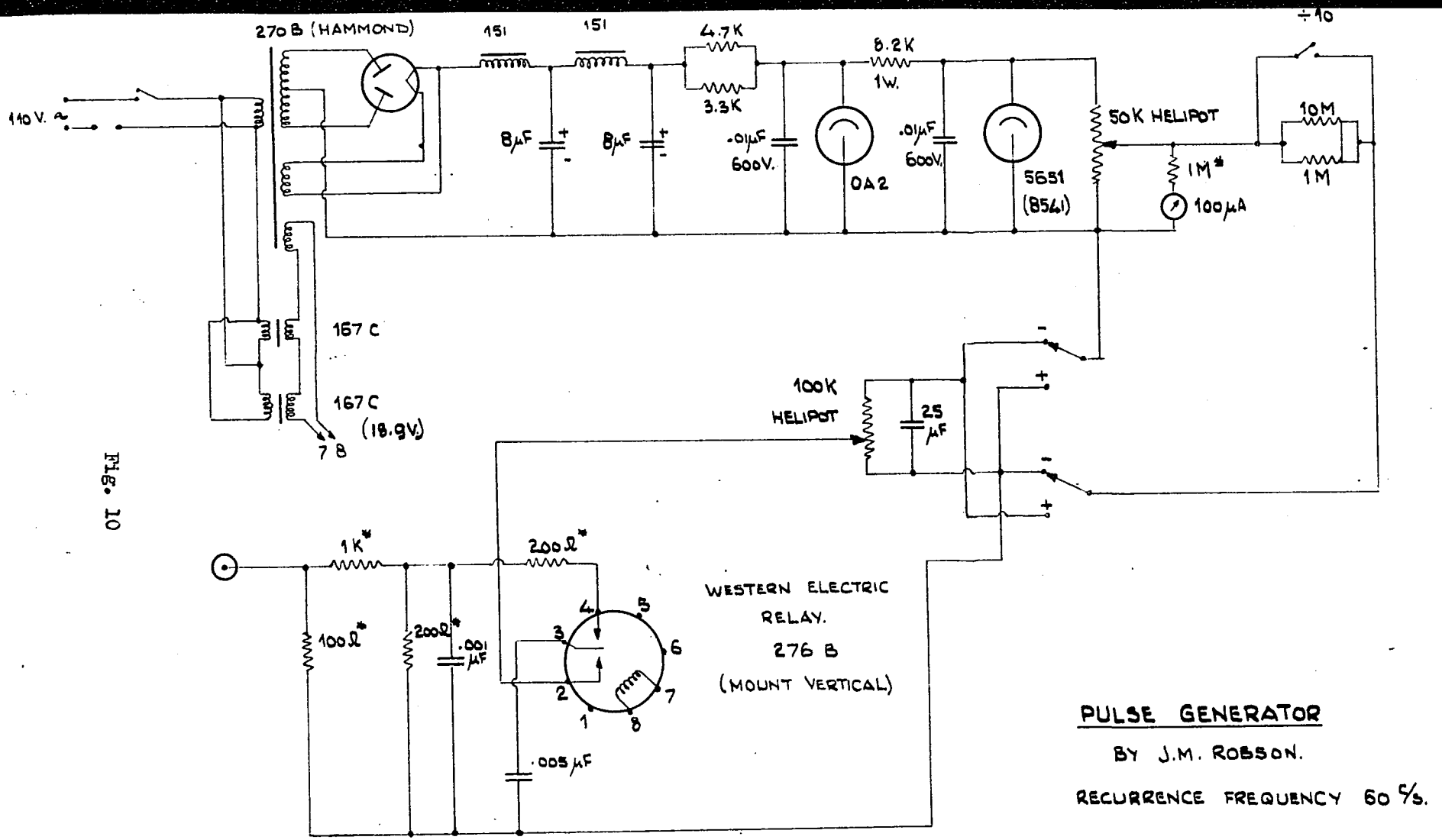

Fig. 10

PULSE GENERATOR

BY J.M. ROBSON.

RECURRENCE FREQUENCY 60 ⁵/s.

certain value below or above a 100V reference voltage. Pulses of either sign can be discriminated. The pulse from the trigger circuit is amplified and fed to a series of 6 scales of two which are of conventional design. The last three stages can be by passed to make a scale of 8. The standard output pulse drives a mechanical register.

The power supply is electronically regulated keeping the voltage constant for 10% variations in either the line voltage or load current.

IV. MEASUREMENTS

A. General

After the spectrometer and associated apparatus have been installed, measurements have to be done in order to calibrate settings and to determine the degree of accuracy which can be attained.

First we carried out relatively simple tests to find:

(i) the resolution of the counter,

(ii) the resolution of the spectrometer,

(iii) the transmission,

(iv) the linearity of the stabilizer setting,

(v) the fluctuation of the stabilizer current.

We used a Cs^{137} and a Tm^{170} source to do the measurements and to compare results with some of the previous work done on these nuclides.

The decay scheme of Cs^{137} is given in fig. 10a. Two modes of beta decay exist: about 8% of the transitions occurs directly to the ground state of Ba^{137} with a maximum beta energy of 1.17 MeV and about 92% of the transitions occur to an excited state of Ba^{137} from which it decays by emission of a .6616 MeV gamma ray in competition with the emission of internal conversion electrons.

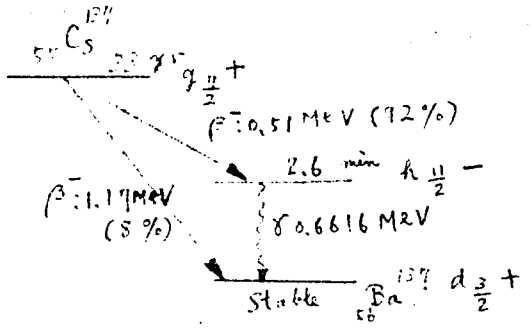

Fig. 18a Decay scheme of Cs^{137}

So far two forms of empirical classification of beta emitters have emerged. One is based on the relationship between the end point energy of the transition and the half period and the other is based on the shape of the beta spectrum (16). The first classification involves logft values. The high energy transition has a partical half life of $\frac{33}{.08}$ ~ 400 yrs, which for an end point energy Wo = 1.17 MeV corresponds to logft = 12.2. The transition is therefore classed as a second forbidden transition with a change in angular momentum $\Delta I = \pm 2$ and no change in parity.

The classification of the shape of the spectrum is by the type of shape correction factor required to multiply the nuclear matrix element in order to obtain a straight Fermi-Kurrie plot. The nuclear matrix element can be visualized physically as representing the degree of overlap of the wave function of the transforming nucleon in its initial and final state.

It is found (17) that the correction factor in the case of the high energy transition confirms the classification by the log ft value. Likewise it is found that the low energy transition is a first forbidden transition with a change of angular momentum of $\Delta I = \pm 2$ and a change of parity.

The gamma decay of Ba^{137*} permits to make an estimate with regard to the value of the angular momentum of this state. The rather long decay half period of 2.6 min indicates a change of several units of angular momentum to the ground state. Furthermore, from the large K conversion coefficient and the small K/L ratio can be concluded that this transition is an M4 transition having the selection rule $\Delta I = 4$, yes (18).

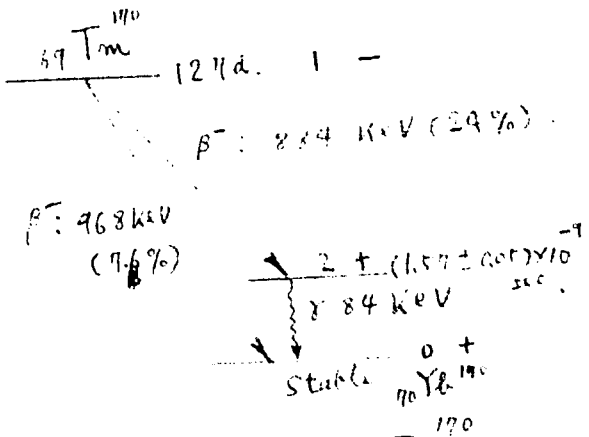

Fig. 16.b Decay scheme of Tm^{170}.

The decay scheme of Tm^{170} is given in fig. 10 b. 76% of the transitions have a maximum energy of 968 KeV, while 24% of the betas have a maximum energy of 884 KeV, leaving the Yb^{170} nucleus in an excited state, 84.4 KeV above ground level. This state decays to the ground state by emission of a gamma ray, found to be an electric quadrupole transition, or by emission of an internal conversion electron.

The log ft values 9.0 and 9.3 for the higher and lower energy transitions respectively suggest that both transitions are first forbidden and involve a change in parity. It is difficult to infer the degree of forbiddenness from the shape of the beta spectra since the Kurie plots yield almost straight lines. However, the high and low energy spectra can be resolved from the gross beta spectrum by using coincidence techniques (14). The shape of the spectrum of the high energy component appears to have a first forbidden shape. It is then assumed from experimental results that the spectrum of the low energy component has also a first forbidden shape.

Returning to the description of the measurements, we used a 5 microcurie Cs^{137} source for the steps (i)-(v).

Then the overall performance of the instrument was checked by taking the full spectrum of a beta emitter. We

used the same Cs^{137} source and a 5 microcurie Tm^{170} source. It was expected to find the end point of the continuous beta spectrum from a Fermi-Kurie plot with an error of less than 7 KeV. Furthermore, the use of the Tm source, which yields K, L, and M lines superimposed upon the continuous spectrum, allows the calculation of the respective conversion coefficients for the lower energy region. Should they agree reasonably well with the known values, then the

spectrometer can be said to perform satisfactorily.

The latter two measurements fall under the headings:

(vi) Resolving the continuous spectrum of Cs^{137},

(vii) Resolving the continuous spectrum of Tm^{170}.

The magnet coil is made up of 4 windings. We used the outer two with which an electron momentum of 5000 gauss-cm can be focussed. The use of only the outer coils decreases the spherical aberration.

It was found that attenuation of the signals in the input of the analyzer to $\frac{1}{4}$ leads to a satisfactory signal input voltage. The high gain of the amplifier otherwise causes overloading in this particular set up

The current in the degaussing coil was maintained at 1.12 Amps, which eliminated the vertical component of the earth magnetic field with an error of less than 1 in 10^3. The direction of the magnet field is opposite to the direction of the horizontal component of the earth magnetic field. This direction was found to give a higher transmission and a better resolution than the North-South direction. We were not able to find an explanation for this phenomenom.

All experiments are run using a slit width in the baffle in the vacuum chamber of $\frac{1}{4}$".

The vacuum was usually better than 2 micron.

The aluminum foil wrapping on the fish eye weighed 600 micrograms/cm^2 at first. It was replaced by a foil weighing 225 micrograms/cm^2 to make recording of the 22.7 KeV, K-peak of Tm^{170} possible. All measurements are taken using the thinner foil except the resolution of the counter at 624 KeV. There is no noticible difference at this energy.

B. Tests

(i) The resolution of the counter

The internal conversion K-peak of Cs^{137} provided monoketic electrons of 624.2 KeV energy. A fixed window of 6%, which value was obtained from the pulse generator by comparison, was superimposed upon the setting of the lower channel. Counts were taken in two minutes intervals. The graphical result is shown in Figure 11. The resolution, being width at half height, is calculated from the graph as 31.3%. - reasonable for this type of counter.

(ii) The resolution of the spectrometer.

Integral bias curves of the Pulse Height Analyzer were taken in order to find a satisfactory plateau setting at various energies, see fig. 12. The best lower bias setting for use with both Cs and Tm source was found to be 138 dial divisions. The output from the lower channel was fed to the scaler. Then the magnet current was varied

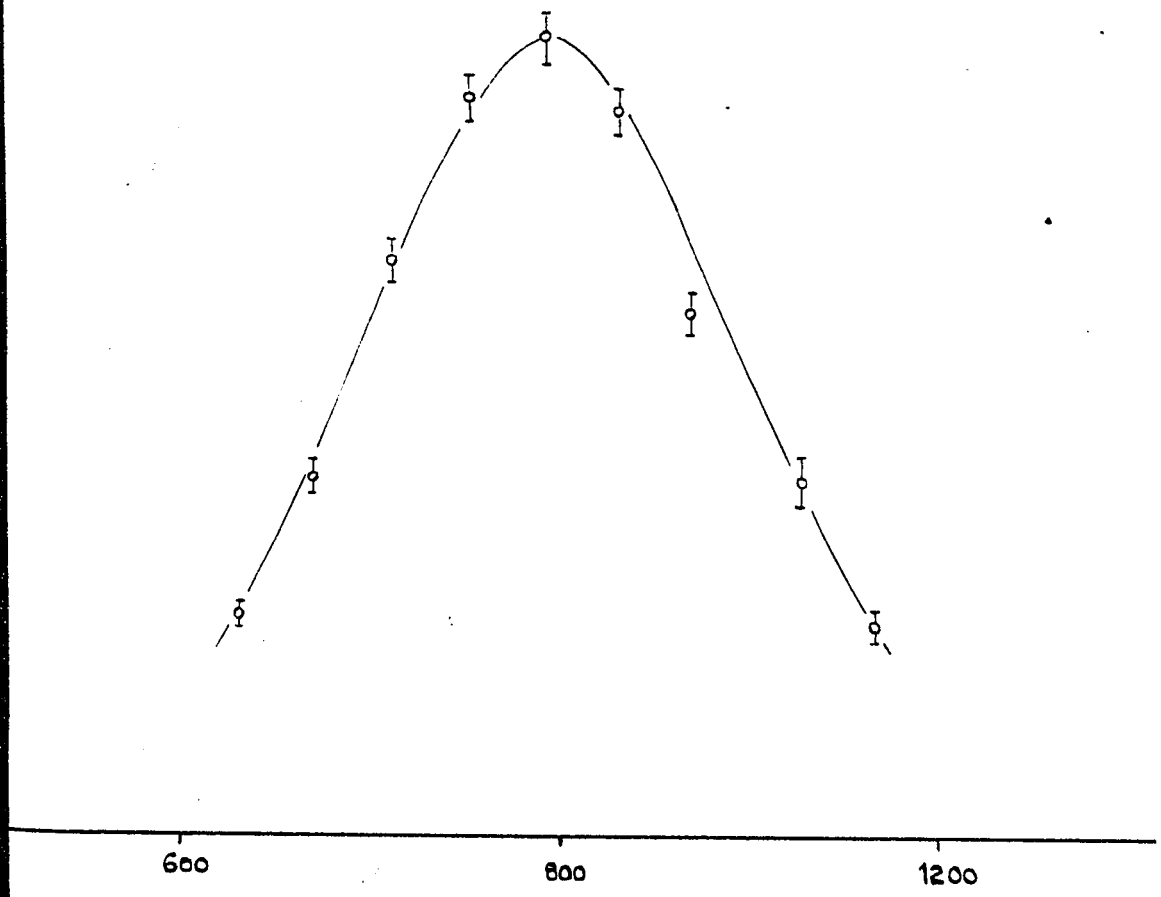

Fig. 11

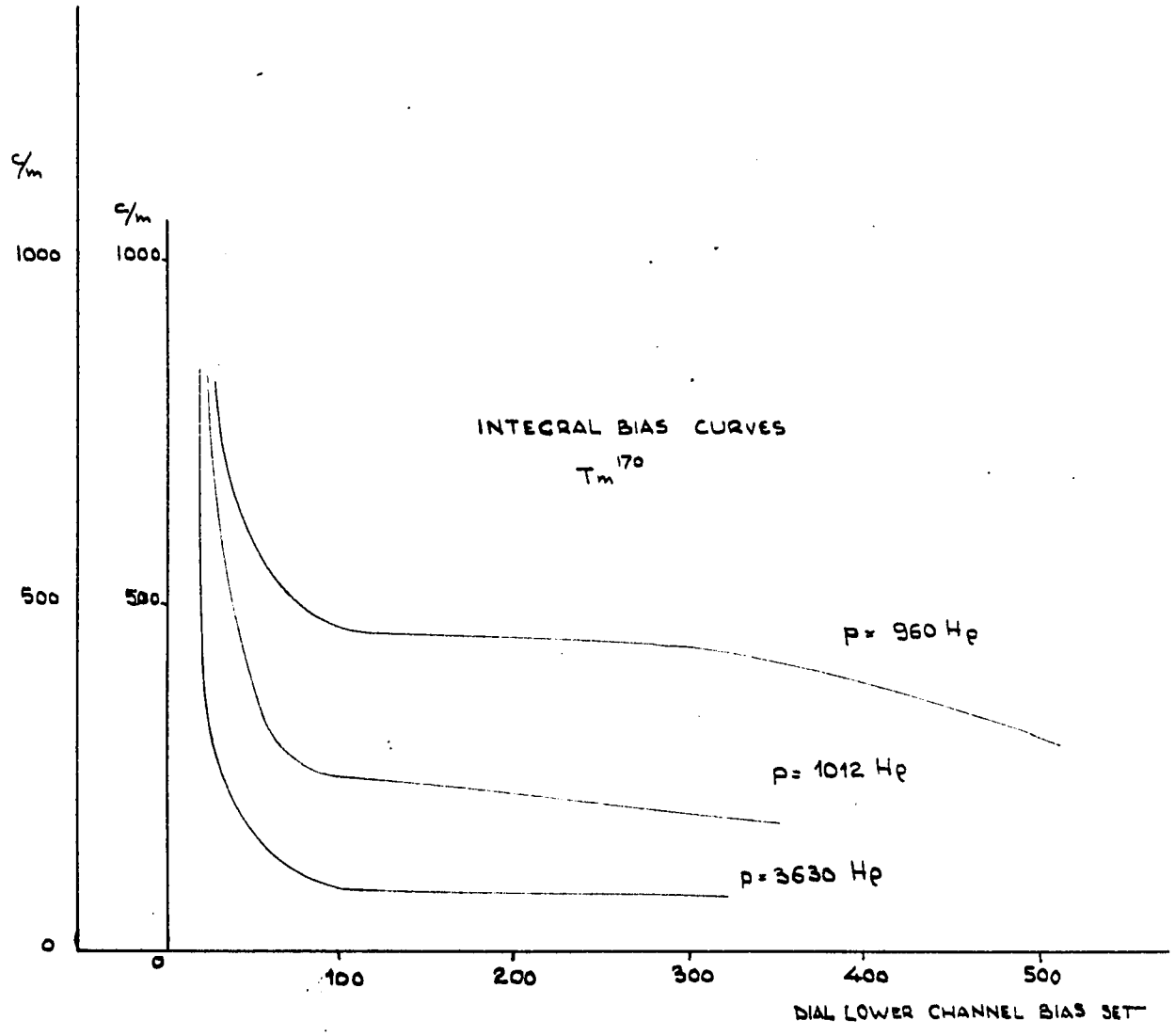
c/m
1000
500
0
c/m
1000
500
0
100
200
300
400
500
INTEGRAL BIAS CURVES
Tm^{170}
p = 960 Hρ
p = 1012 Hρ
p = 3630 Hρ
DIAL LOWER CHANNEL BIAS SET

Fig. 12a

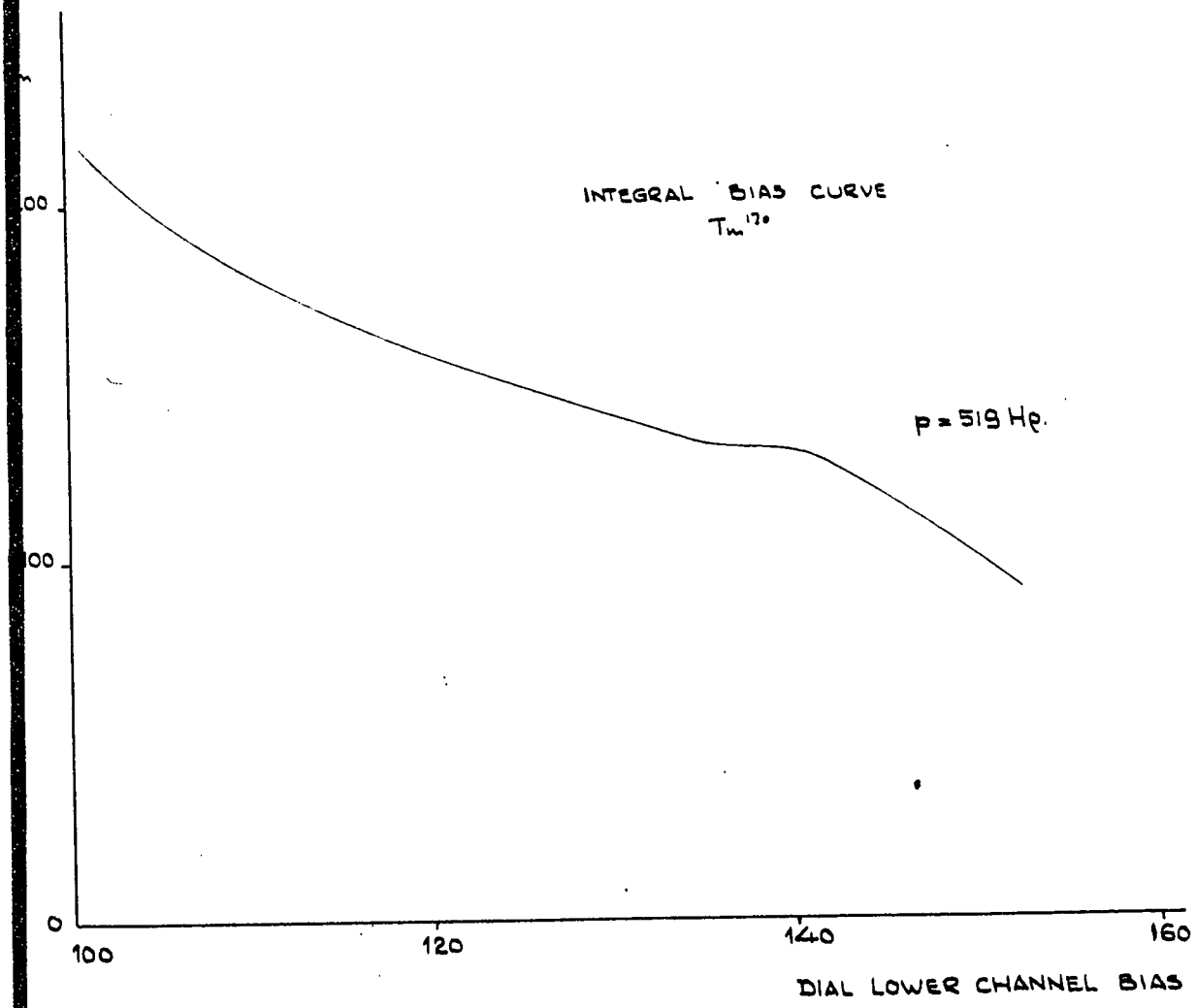
INTEGRAL BIAS CURVE
T_m 170
p = 519 Hp.
00
00
0
100
120
140
160
DIAL LOWER CHANNEL BIAS

Fig. 12b

over the range of the peak. The resolutions at half height of the Cs K peak and the Tm L peak are 2.16% and 2.6% respectively; the higher value of the latter determination due to the combination of L II and L III electrons into one peak.

The resolution at half height is theoretically:

$$R = \frac{ms+w}{2(m+1)d} \qquad (13)$$

Assuming a triangular resolution curve by approximation:

$$R = \frac{(1x1 + 2.75)x100}{2(1+1) \times 3.125 \times 25.4} = 1.5\%$$

(iii) Transmission

Again using the K-peak of Cs^{137}, then the number of electrons emitted per min is:

$$N = \text{strength in curies} \times 60 \text{ mins} \times \alpha_K \text{ electrons/min} \qquad (17)$$

$$= 5 \times 3.7 \times 10^4 \times 60 \times .1$$

$$= 11.1 \times 10^5/\text{min.}$$

Max Counting rate is 2350 c/m, hence the fractional solid angle is:

$$T = \frac{2350 \times 100}{11.1 \times 10^5} = .21\%$$

The transmission is given by the geometry as:

$$T = \frac{d \times \Delta d}{2u^2} \qquad (15)$$

Whereby $w = m \times s$

$$= \frac{3.125 \times 25.4 \times 6.3 \times 100}{2 \times 422^2} = .14\%$$

In our case the radius of the detector window is much larger than $m \times s$, which explains the discrepancy between experimental and theoretical value.

(iv) Linearity

As explained in the discussion of the magnet stabilizer, the reference voltage for the chopper is taken from dry cells by means of a 10 turn helipot.

Using the Cs^{137} source, the difference between K and L lines is:

$$\frac{|K - L|}{K} = \frac{653.3 - 676.2}{653.3}$$

= 3.51% as expressed in dial settings.

The value given by the actual momenta is 3.52%. The dial settings, however, cannot be calibrated absolutely until the reference voltage is taken from or compared to the voltage from Weston Standard cells.

(v) Fluctuation of magnet current

An oscilloscope was calibrated with a low A.C. voltage and then connected to the ½ Ohm resistor in the magnet current line. The voltage fluctuations were converted into units of current and appeared to be less than .02% of the nominal magnet current.

(vi) Resolving the continuous spectrum of Cs^{137}

The full spectrum is given in fig. 12 and the corresponding Fermi-Kurie plot in fig. 13.

Both plots are corrected for the continous background spectrum, which consists of a straight line through the counts per minute at $H\rho = 0$ and at $H\rho = 3640$ gauss-cm. Also resolution correction is applied to the end region of the continuous spectrum. This correction is given by G.E. Owen et al (13) as:

$$n(p) = m(p) - \frac{a^2}{4}\left(\frac{d^2m}{dp^2}\right)_p \qquad (18)$$

where:

n(p) = true count

m(p) = observed count

a = half width at half height

An energy dependent correction factor is applied to the Fermi-Kurie plot in order to obtain a straight line (8).

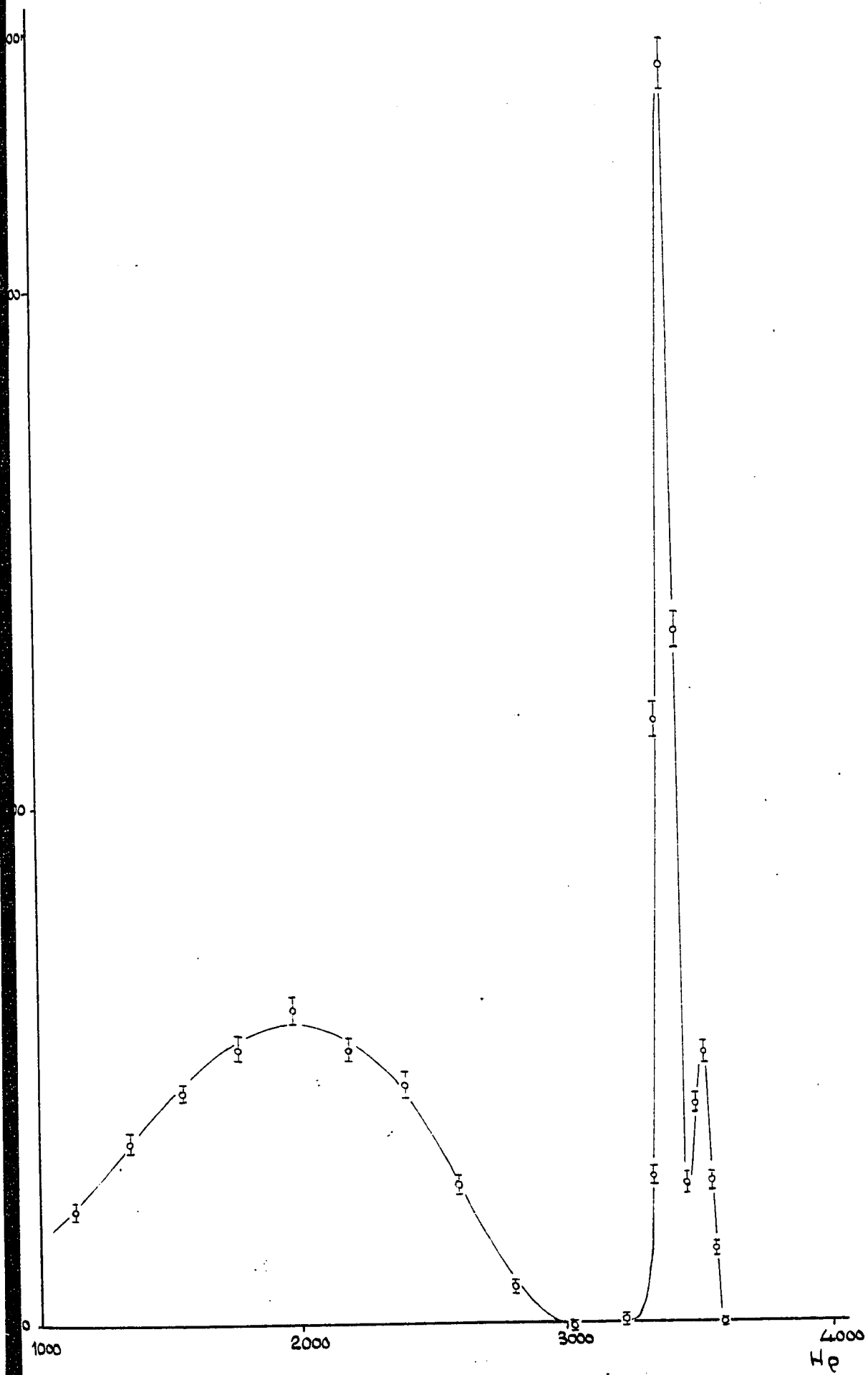

Fig. 12

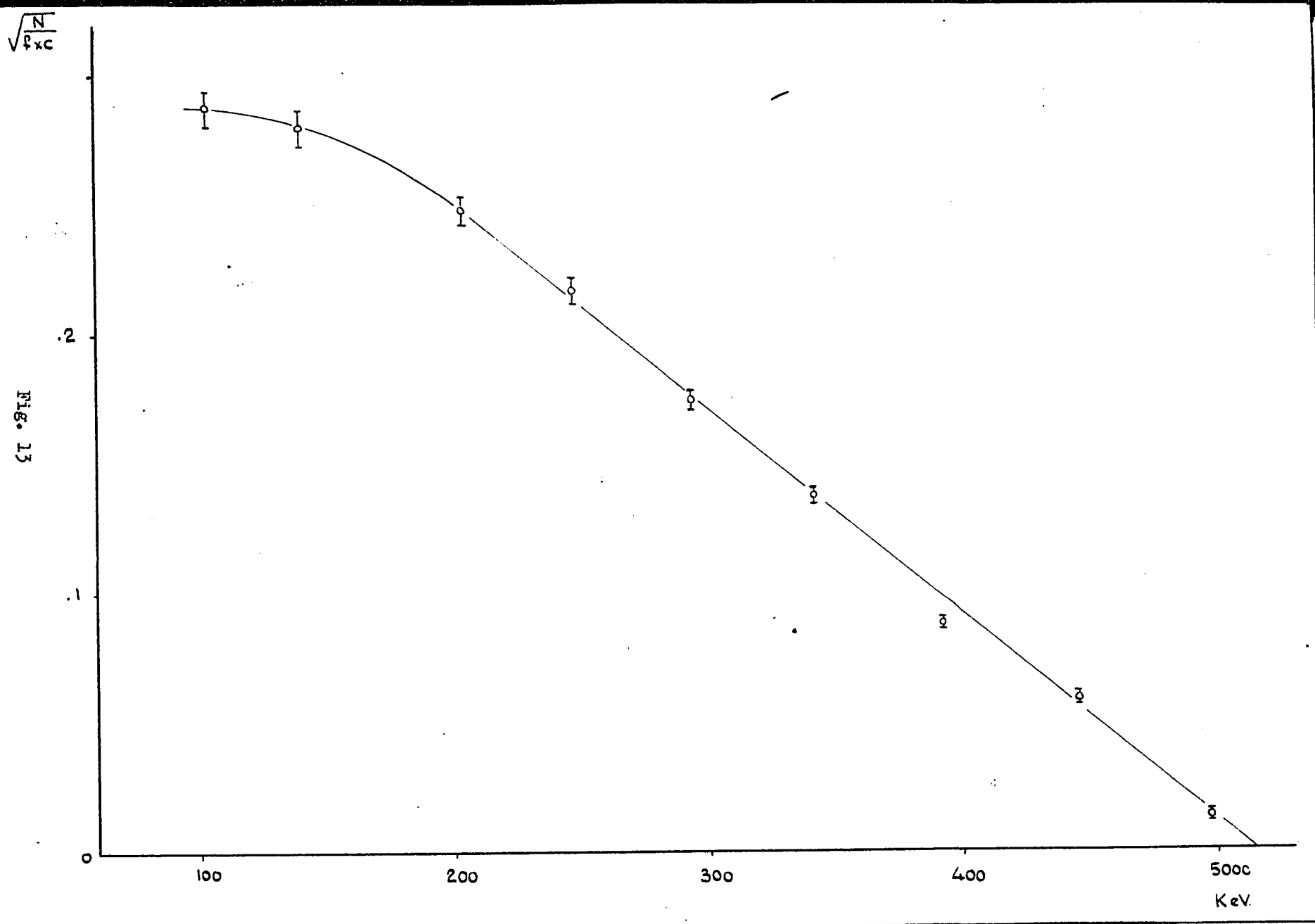

Fig. 13

This factor is for a Gamow-Teller first forbidden transition, as in the case of the 92% low energy transition of Cs^{137}:

$$C_1 = (W^2-1) \div (W_o-W)^2 \qquad (19)$$

where:

W: the kinetic energy of the electron in absolute units

$$W = \frac{E+m_oc^2}{m_oc^2}$$

$$= \frac{E(MeV)}{0.51} + 1 \qquad (20)$$

W_o: the end point of the beta spectrum in absolute units

$W_o = \frac{523 \div 511}{511} = 2.022$ for the low energy transition of Cs^{137}.

The end point as found from the Fermi-Kurie plot is 514 ± 5 KeV. R.D. Evans gives .51 MeV.

The drooping in the F.K. plot below 150 KeV is to be expected from the foil thickness and from the source thickness.

(vii) Resolving the continuous spectrum of Tm^{170}

First a remark has to be made with regard to the integral bias curves, fig. 11. As was to be expected, a counter plateau for K peak electrons could hardly be seen. We therefore resorted to calibration of the lower channel bias by means of the pulse generator. It was first set to give pulses comparable to pulses from L peak electrons and then it was set to give pulses comparable to a K/L fraction of the energy of the L peak electrons. The mid-point of the plateau was thus found and we only had to take counts in its vicinity to determine its exact location. There appeared to be no appreciable difference with the setting calibrated from the pulse generator.

The full spectrum is shown in fig. 14 and the Fermi-Kurie plot in fig. 15. The correction for background is applied to both curves, the correction for spectrometer resolution is applied to the calculations for the F-K plot only.

The Fermi-Kurie plot is very nearly a straight line. An inflection at about 965 KeV could no doubt have been shown if coincidence techniques could have been used. Time, however, did not permit this. The end point is found to be 977 $\pm$ 9 KeV. Graham et al give 968 KeV.

K, L, and M ratios are determined from the respective areas under the peaks plotted as counting rate per unit

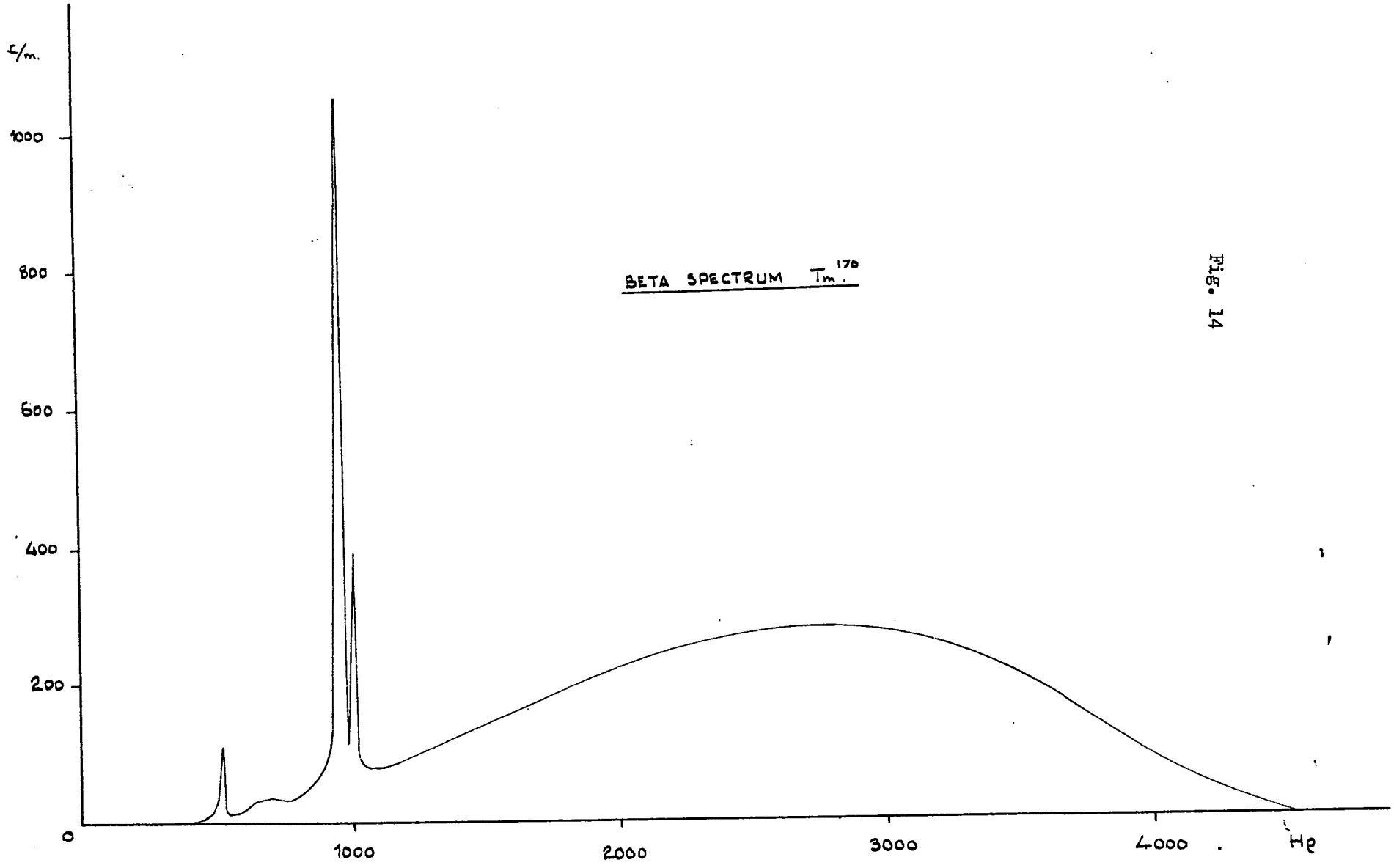

BETA SPECTRUM Tm^{170}.

Fig. 14

Fig. 15

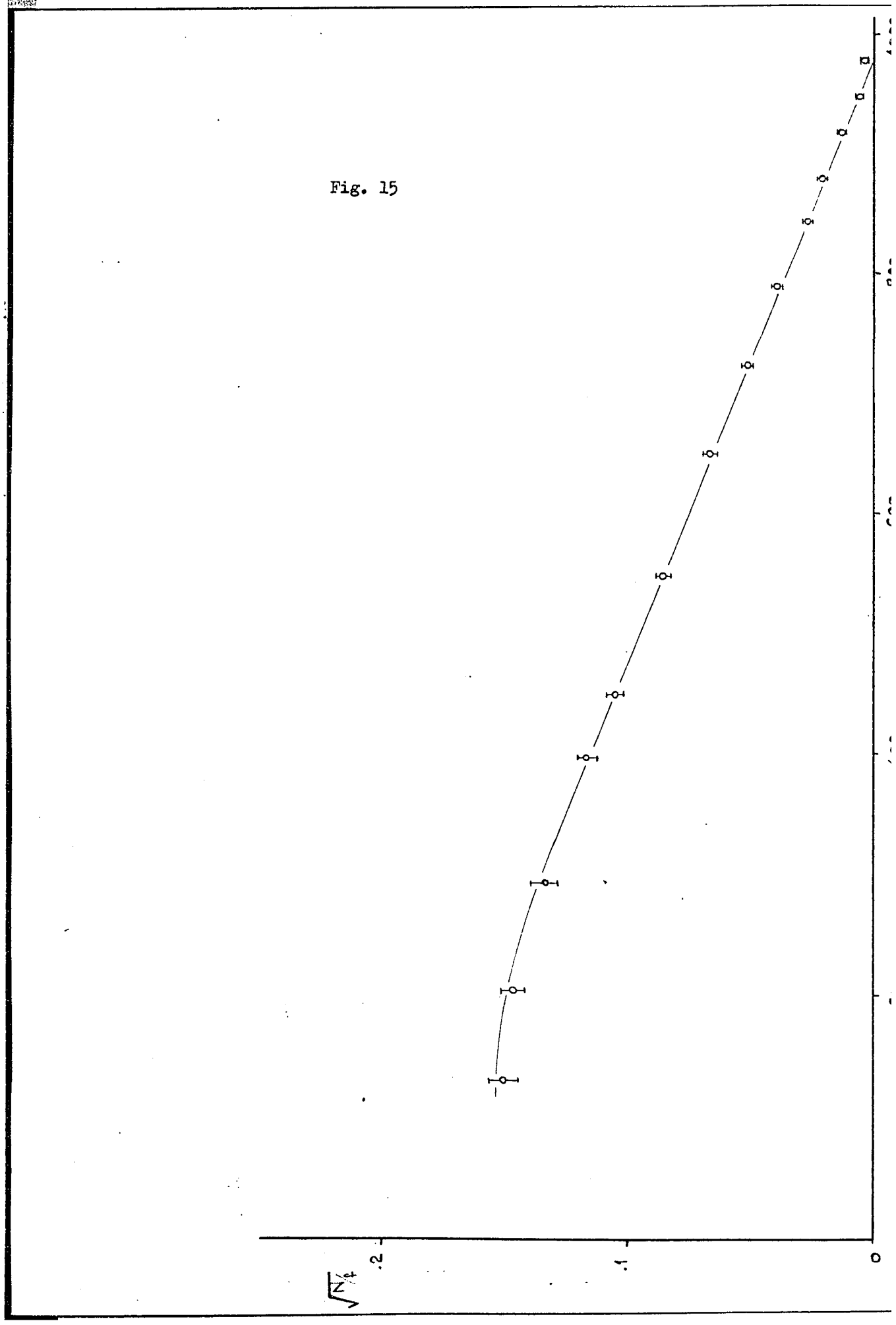

momentum vs momentum. The ratios determined by Gray and by Graham et al are also given.

Ratio	Gray	Graham	We
K:L:M	100:314:72	100:360:-	100:785:245
L:M:K	100:22.9:32	100: - :27.8	100:32:12.7
M:L:K	100:139:436	-	100:~~40.7:330~~ 320:40.7

The K/L and the L/M values are much lower than the values obtained by Gray and Graham et al. This is almost certainly due to absorption in the 225 microgram foil over the counter resulting in a loss of counts which is more pronounced at lower energies.

The internal conversion coefficient for L electrons, α_L, is given by:

$$.24 \frac{N_E}{N_L} = 1 + \frac{K}{L} + \frac{M}{L} + \frac{1}{\alpha_L} \qquad (21)$$

Where N_E, N_L and the ratios are obtained from the respective areas under the curve of counting rate per unit momentum vs momentum.

Hence:

$$0.24 \times 10.9 = 1 + .127 + .313 + \frac{1}{\alpha_L}$$

$$\alpha_L = .845$$

Graham et al gives a value of 4.1.

V CONCLUSIONS

The values of both resolution and transmission of the spectrometer are higher than might be expected from geometrical considerations. This is due to the difference in ratios of E/S = 2.75 and u/v = m = 1. The counter window absorbs thus not only electrons of the proper momentum but also electrons of slightly different momentum. The ratio of u/v should be decreased to 1/2.75 in order to match the counter window to the source area. The transmission however, will not change very much because it was measured on monokinetic electrons.

Deutsch et al, however, points out that the most satisfactory values for both transmission and resolution are obtained at a magnification of one. In our case better results would probably have been obtained if we had used aluminum rings to decrease the effective counter window.

The linearity of the stabilizer settings and the small value of the fluctuations in the magnet current are satisfactory, although there is still room for improvement by the use of the already mentioned Weston cells and probably by a more careful adjustment of the stabilizer.

The following can be said with regard to the L line conversion coefficient. As remarked above, the foil

over the counter has very likely been too thick. We will therefore assume our K/L ratio to be in error, due to incomplete counting of K electron counts by the counter. Hence we take the value of N_E/N_L from our experimental data and the K/L and M/L values from Graham et al.

We estimate the errors as follows:-

(i) The factor 0.24 which gives the fraction of the decays of Tm^{170} which lead to the excited state of Yb^{170}, is taken from the work of Graham et al, where it was obtained by a coincidence technique. Other workers have obtained 0.22. We therefore take $\pm$ .02 as the error in this quantity.

(ii) The ratio $\frac{N_E}{N_L}$ is obtained by taking a ratio of areas and is subject to uncertainty in estimating the area at the base of the L peak and of the continuum at the low energy end. Estimates from our data on different assumptions indicate an error of $\pm$ 1.5 in this ratio.

(iii) The error in K/L is taken from the work of Graham et al as $\pm$ .04.

(iv) The error in M/L is estimated as $\pm$ .04.

Hence,

$$(.24\pm.02) \times (10.9\pm1.5) = 1 + (0.36\pm.04) + (0.31\pm0.4) + \frac{1}{\alpha_L}$$

giving

$$\alpha_L = 1.05^{+2.08}_{-.45}$$

This value is in disagreement with that obtained by Graham et al who used an absolute counting technique. We

would expect our value to be low due to:-

(i) Possible loss of L conversion electrons in the source. There is some evidence for this in the pronounced low energy tail on the L line.

(ii) Non perfect alignment of the spectrometer. This would be more serious at low energies than at high energies and would tend to make our observed value of N_L/N_K low.

(iii) Possible loss of L conversion counts in the counter. This is not expected to be serious as the bias curve appeared to be very flat at this energy.

To resolve this discrepancy further work would be necessary involving a redetermination with a thinner source. The time available for this work (3 months) has not permitted us to investigate this. We conclude that there may be some doubt as to the published values of the α_L for Tm^{170} but further work is required to establish this.

As to the performance of the spectrometer, it may be concluded that this instrument certainly permits the investigator to obtain reliable figures over a wide range of particle energies provided some more work is done on improvement of the resolution and use is made of the provision for coincidence counting where applicable.

VI ACKNOWLEDGEMENT

I would like to express my gratitude to Mr. J.M. Robson, who could see us only once a week, but then untiringly rendered us all the assistance we asked for.

I feel also very much in debt to my fellow worker, Mr. Y. Motoda, with whom I spent a most pleasant and fruitful summer at the University of Ottawa.

Furthermore, I would like to thank the staff of the Physics Department and especially Prof. G. Lamarche who generously contributed to our results with ideas and materials.

BIBLIOGRAPHY

(1) J.M. Robson: Phys. Rev. 83, (1951), 349.

(2) K. Siegbahn: "Beta and Gamma Ray Spectroscopy", Chap. III, Interscience Publishers, 1955.

(3) H. Slätis: Ark. F. Fysik 8, No. 43, (1954) 441.

(4) H. Busch: Ann. Physik 81, (1926) 974.

(5) M. Deutsch, L.G. Elliot and R.D. Evans: Rev. Scint. Instr. 15, (1944), 178.

(6) W. Pratt, F. Boley and R. Nichols: Rev. Scient. Instr. 22, (1952) 92.

(7) Y. Motoda: Thesis, Ottawa University.

(8) R.D. Evans: "The Atomic Nucleus", Chap. 21, Sec 3 Chap. 17, McGraw-Hill, (1955).

(9) L. Katz, A.S. Penfold: Rev. Mod. Phys. 24, (1952) 28.

(10) W.C. Elmore and M. Sand: "Electronics", Chap. II, Sec. 4,3, McGraw Hill, (1949).

(11) J.M. Robson: Notes on Nuclear Physics, University of Ottawa.

(12) I. Kaplan: "Nuclear Physics", Chap. 14, Sec. 4-6, Addison-Wesley, (1956).

(13) G.E. Owen and H. Primakoff: Phys. Rev. 74 (1948) 1406.

(14) R.L. Graham, I.L. Wolfson and R.E. Bell: Can. J. Phys. 30, (1952) 459.

(15) P.R. Gray: Phys. Rev. 101, (1954) 1523.

(16) E.J. Konopinski: Revs. Mod. Phys. 15 (1943) 209.

(17) L.M. Langer and R.J.D. Moffat: Phys. Rev. 82 (1951) 635.

(18) M.A. Waggoner: Phys. Rev. 82 (1951) 906.

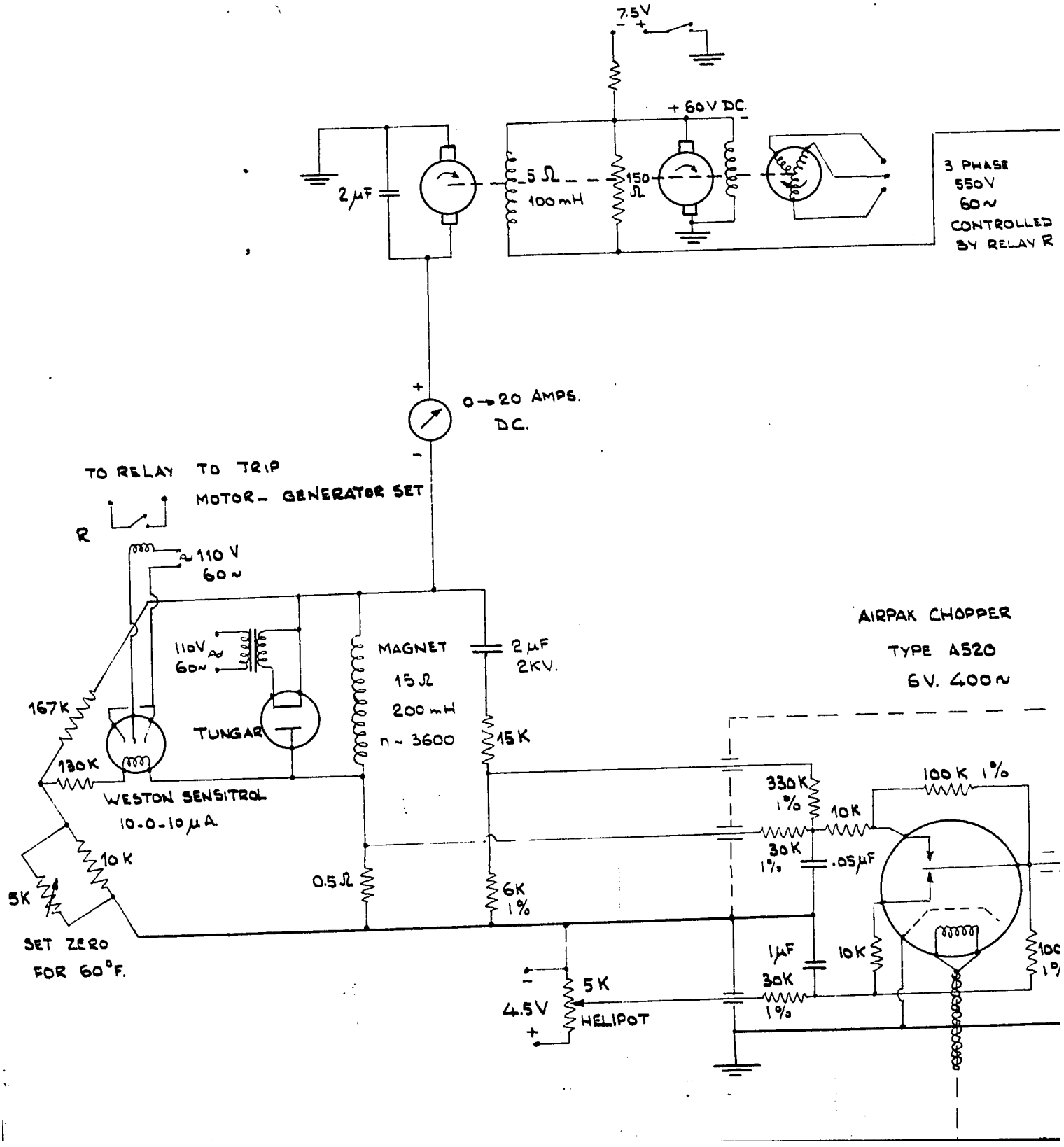
7.5V
+ 60V DC.
2 μF
5 Ω
100 mH
150 Ω
3 PHASE
550V
60~
CONTROLLED
BY RELAY R
0 → 20 AMPS.
DC.
TO RELAY TO TRIP
MOTOR - GENERATOR SET
R
~110 V
60~
110V ~
60~
MAGNET
15 Ω
200 mH
n ~ 3600
2 μF
2KV.
167K
TUNGAR
15K
130K
WESTON SENSITROL
10-0-10 μA.
10K
5K
SET ZERO
FOR 60°F.
0.5 Ω
6K
1%
AIRPAK CHOPPER
TYPE A520
6V. 400~
330K
1%
10K
100K 1%
30K
1%
.05μF
1μF
10K
30K
1%
5K
4.5V
HELIPOT

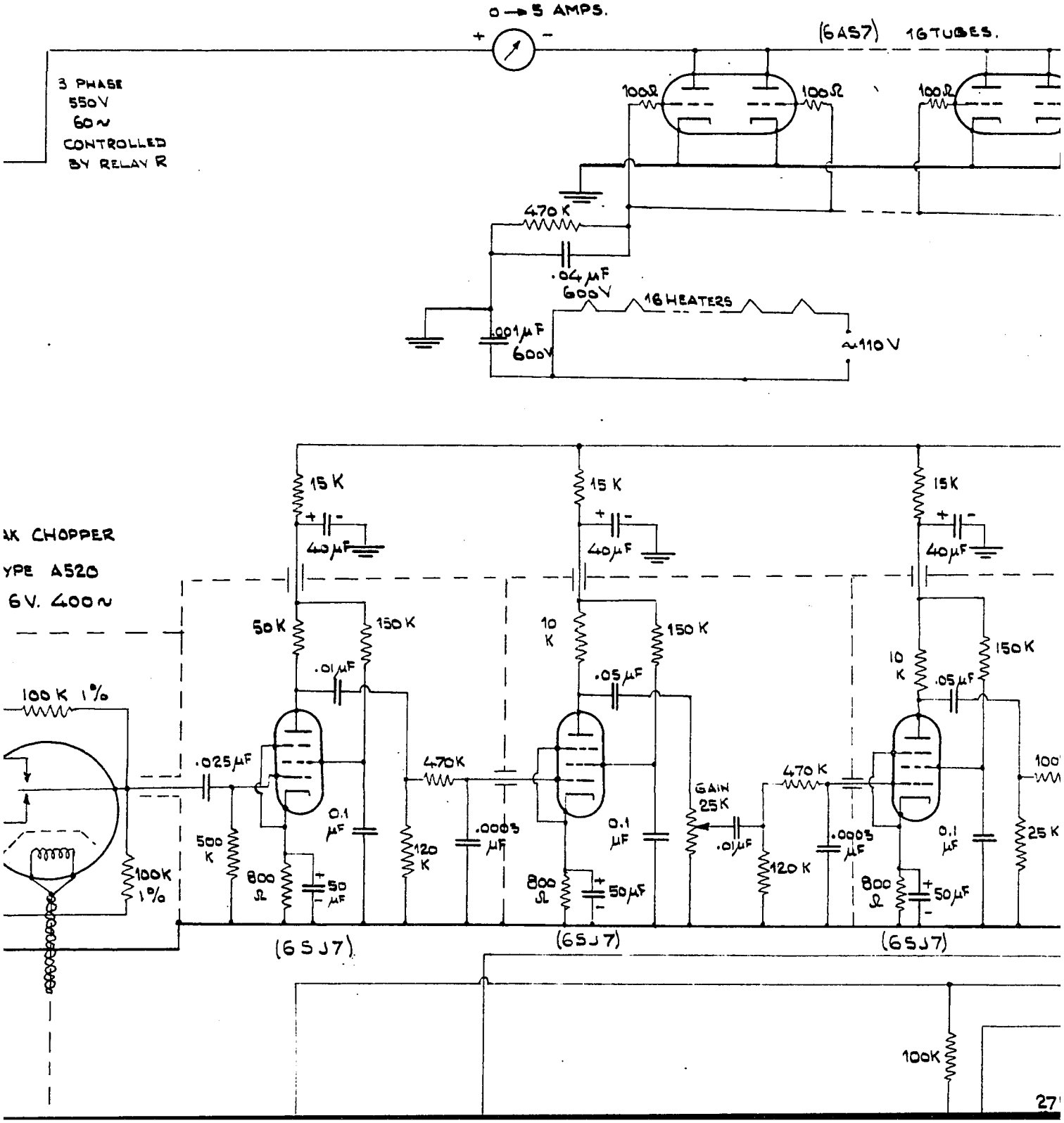
0 → 5 AMPS.
+
−
(6AS7) 16 TUBES.
3 PHASE
550V
60~
CONTROLLED
BY RELAY R
100Ω
100Ω
100Ω
470 K
.04 μF
600V
16 HEATERS
.001 μF
600V
~110 V
15 K
40 μF
50 K
150 K
.01 μF
10 K
.05 μF
100 K 1%
.025 μF
470K
0.1 μF
500 K
800 Ω
50 μF
120 K
.0005 μF
GAIN
25K
.01 μF
25 K
100K 1%
(6SJ7)
100K

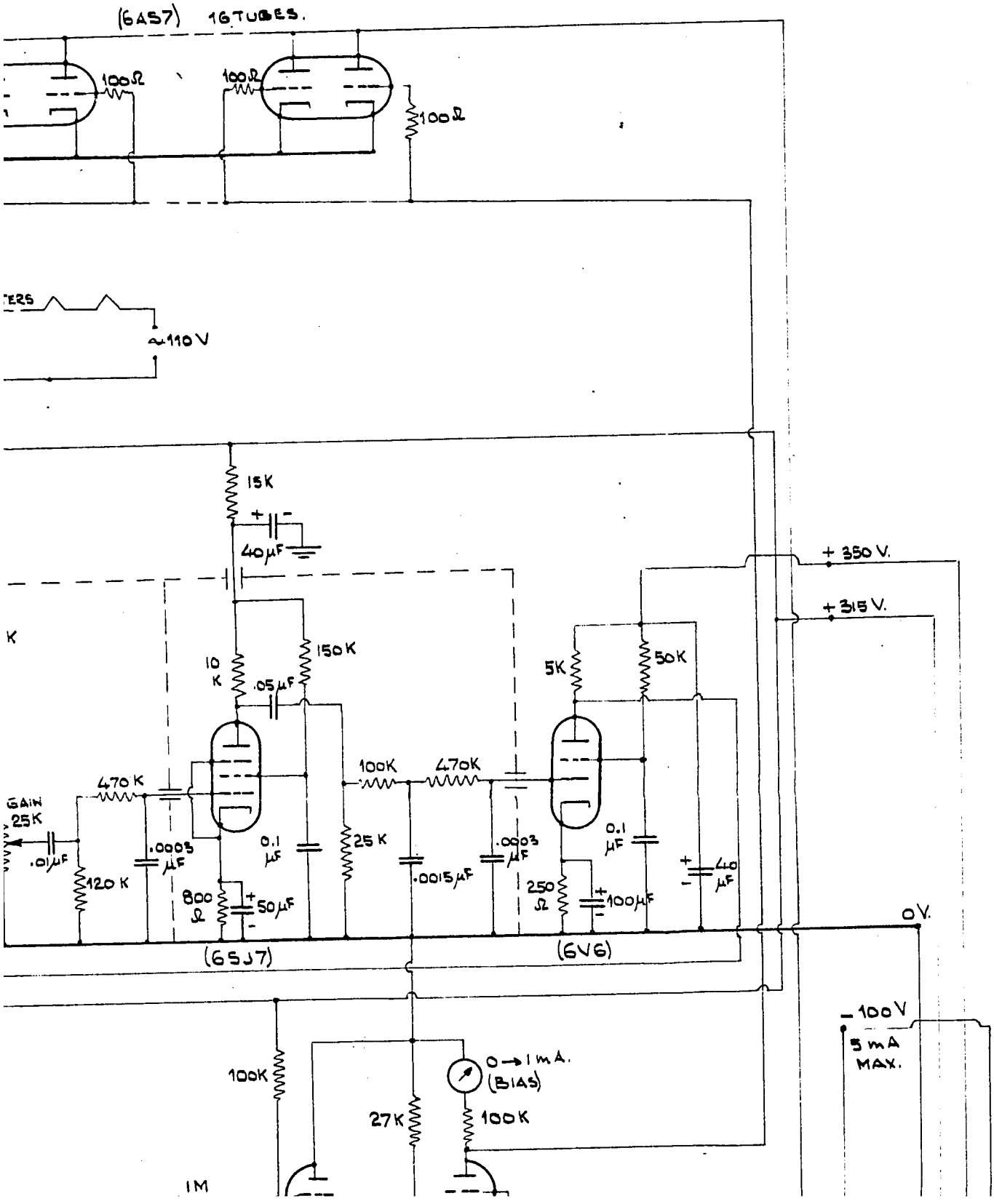
(6A57) 16 TUBES.
100Ω
100Ω
100Ω
~110 V
15K
40μF
+ 350 V.
+ 315 V.
10 K
.05μF
150K
5K
50K
470K
100K
470K
GAIN 25K
.01μF
120K
.0003 μF
0.1 μF
800 Ω
50μF
25K
.0015μF
.0003 μF
0.1 μF
250 Ω
100μF
40 μF
0V.
(6SJ7)
(6V6)
100K
0 → 1 mA. (BIAS)
27K
100K
- 100 V
5 mA MAX.
1M

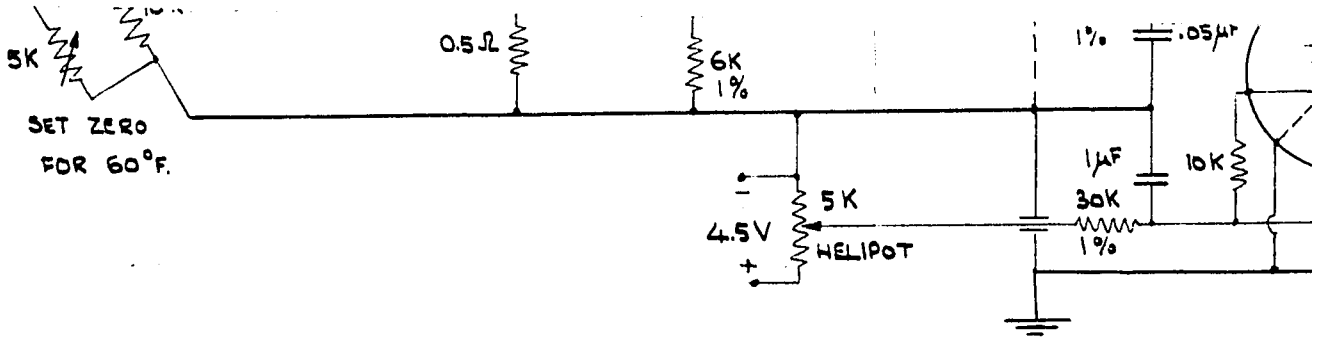

BETA SPECTROMETER

MAGNET STABILIZER.

ORIGINALLY USED FOR THE NEUTRON
LIFE TIME EXPERIMENT.

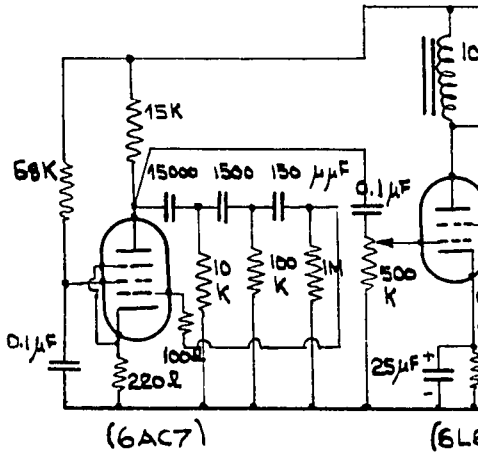

T_1 : HAMMOND # 333.

T_2: " # 344.

T_3: " # 270.

ADJUST TO
6.3 V 400
A → GRO

SEPT. 2/57
dwf.

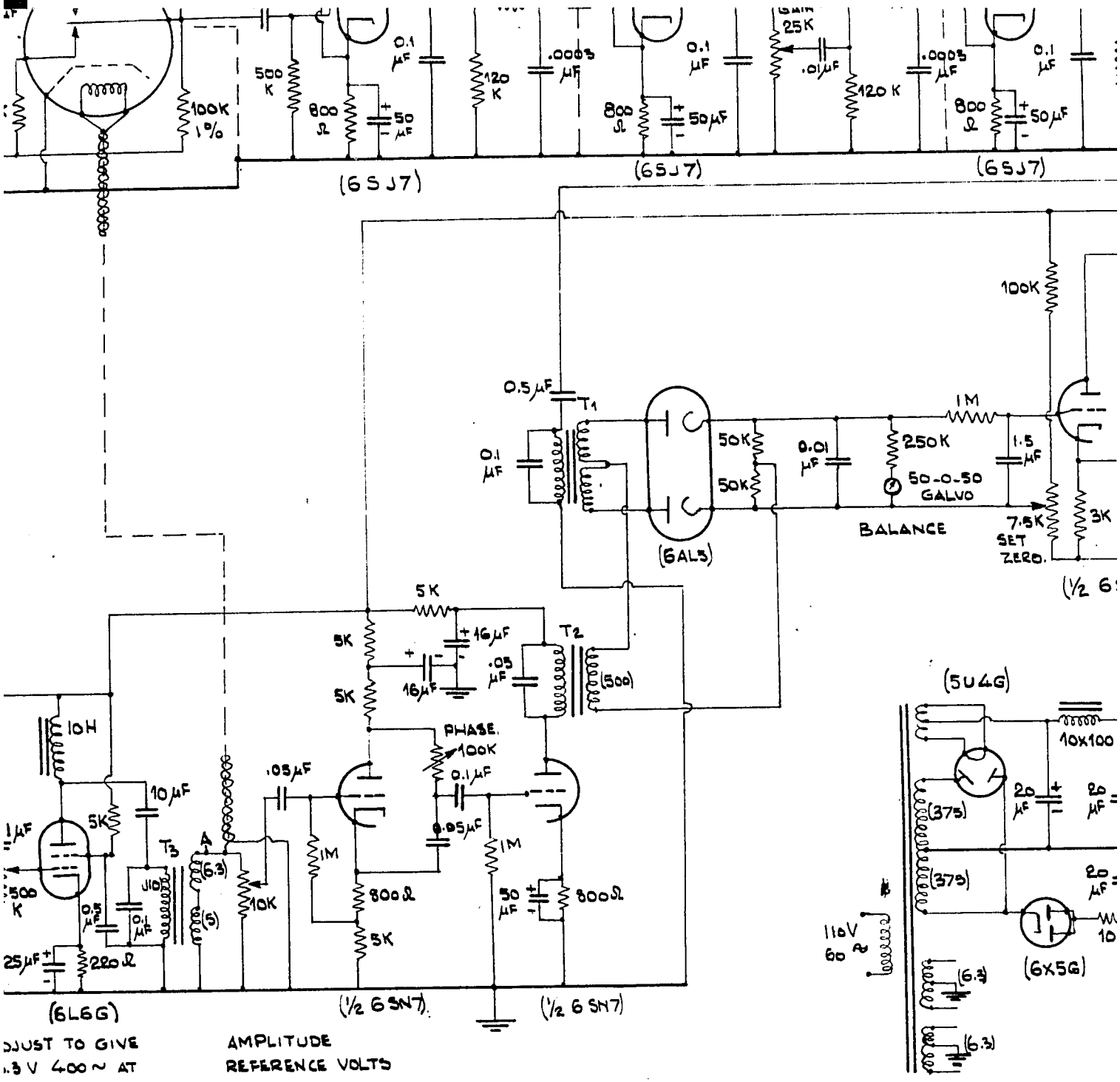
100K 1%
500 K
800 Ω
0.1 μF
50 μF
120 K
.0005 μF
(6SJ7)
GAIN 25K
.01μF
0.5μF
T1
0.1 μF
50K
50K
0.01 μF
250K
50-0-50 GALVO
BALANCE
1M
1.5 μF
7.5K SET ZERO.
3K
100K
(6AL5)
(½ 6
5K
5K
5K
16μF
16μF
.05 μF
T2
(500)
PHASE.
100K
0.1μF
.05μF
.05μF
1M
1M
800Ω
800Ω
5K
50 μF
10H
10μF
5K
T3
(6.3)
A
(5)
10K
.1μF
500 K
.5 μF
.01 μF
.25μF
220Ω
(6L6G)
(½ 6SN7)
(½ 6 SN7)
(5U4G)
10x100
20 μF
20 μF
(375)
(375)
110V 60 ~
(6X5G)
(6.3)
(6.3)
DJUST TO GIVE
.3 V 400 ~ AT
A → GROUND
AMPLITUDE
REFERENCE VOLTS

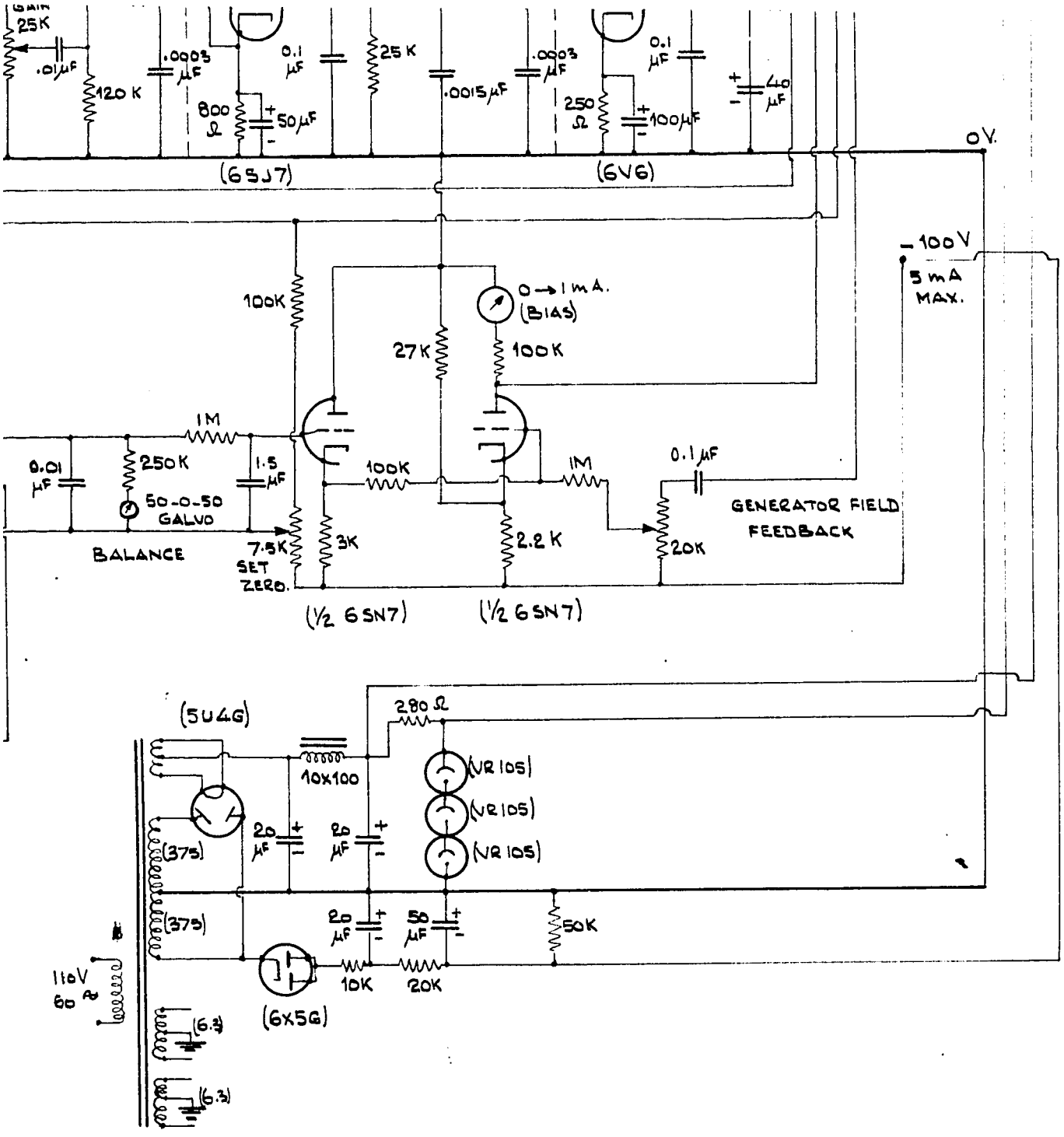
GAIN 25K
.01 μF
120 K
.0003 μF
800 Ω
0.1 μF
50 μF
25 K
.0015 μF
.0003 μF
250 Ω
0.1 μF
100 μF
40 μF
0 V.
(6SJ7)
(6V6)
100K
0 → 1 mA.
(BIAS)
27 K
100K
-100 V
5 mA MAX.
1M
0.01 μF
250K
50-0-50 GALVO
1.5 μF
100K
1M
0.1 μF
GENERATOR FIELD FEEDBACK
BALANCE
7.5K SET ZERO.
3K
2.2 K
20K
(½ 6SN7)
(½ 6SN7)
(5U4G)
280 Ω
10x100
(VR 105)
(VR 105)
(VR 105)
20 μF
20 μF
(375)
(375)
20 μF
50 μF
50K
10K
20K
(6X5G)
110V 60 ~
(6.3)
(6.3)

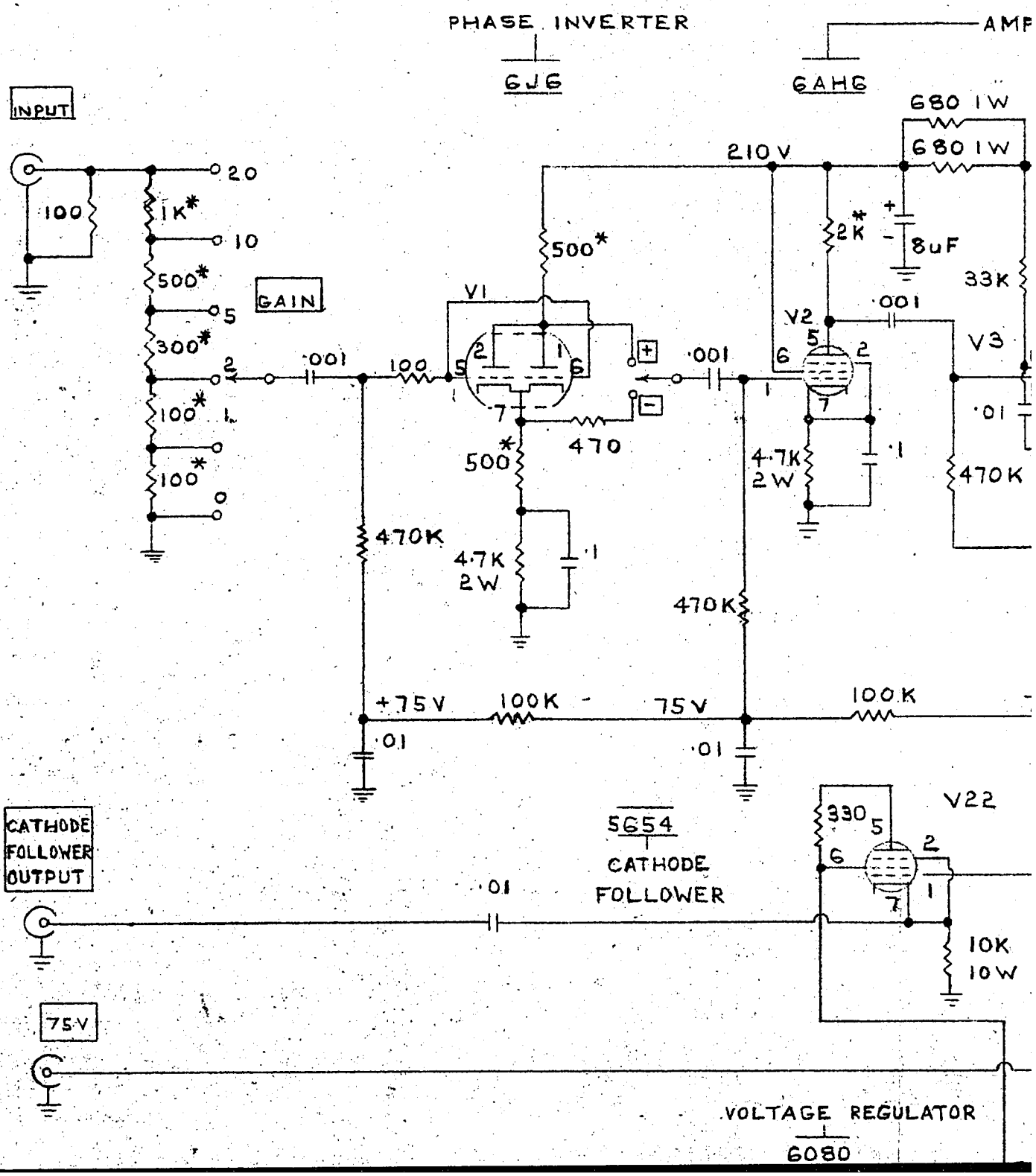
PHASE INVERTER
6J6
AMP
6AH6
INPUT
680 1W
680 1W
210V
100
1K*
20
10
500*
5
300*
2
100*
1
100*
0
GAIN
.001
100
V1
500*
2K*
8uF
33K
.001
V2
V3
.001
470
500*
4.7K
2W
.1
470K
.01
470K
4.7K
2W
.1
470K
+75V
100K
75V
100K
.01
.01
CATHODE
FOLLOWER
OUTPUT
5654
CATHODE
FOLLOWER
V22
330
.01
10K
10W
75V
VOLTAGE REGULATOR
6080

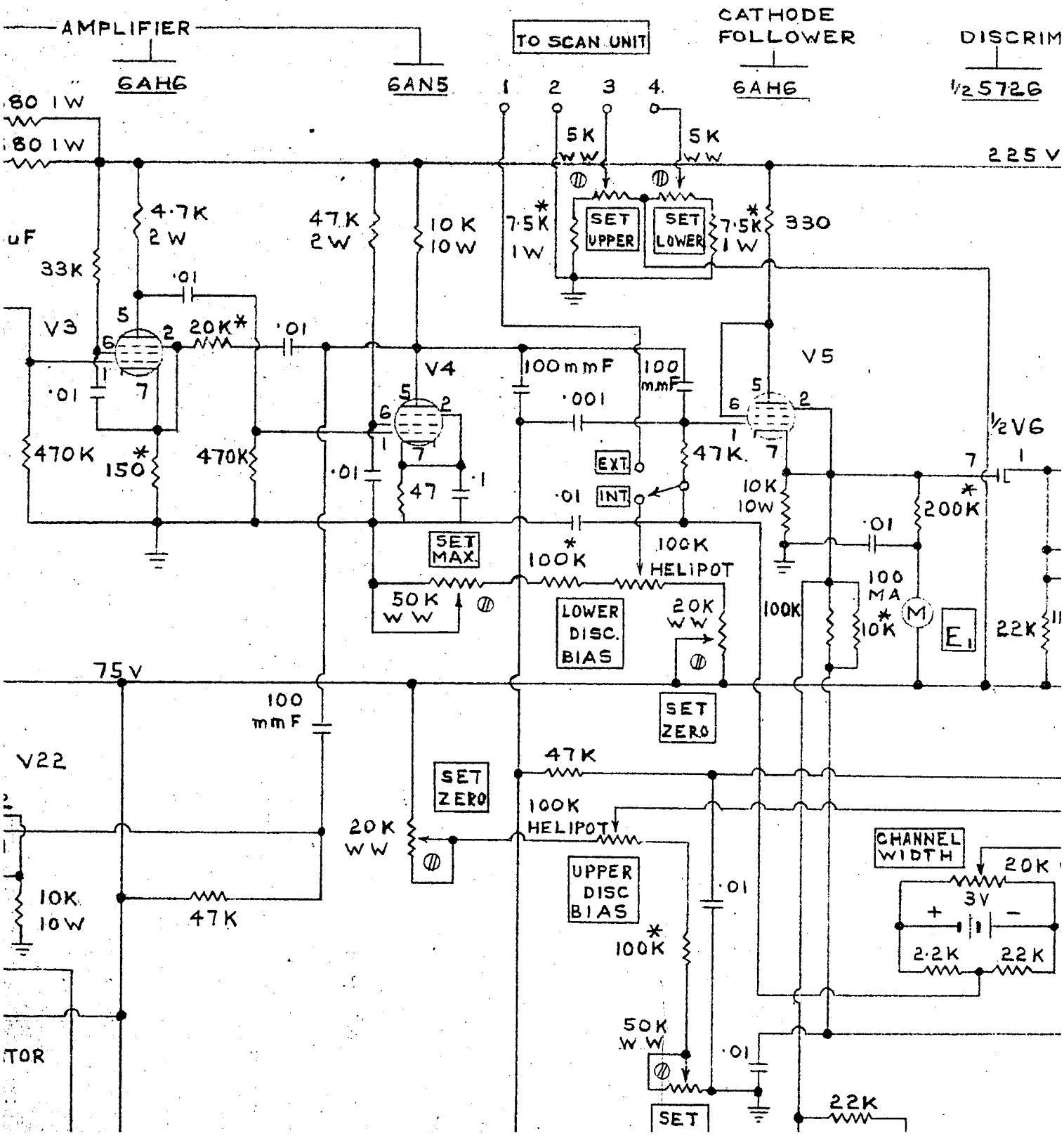
AMPLIFIER
6AH6
6AN5
TO SCAN UNIT
1 2 3 4
CATHODE FOLLOWER
6AH6
DISCRIM
½5726
80 1W
80 1W
5K WW
5K WW
225 V
4.7K 2W
47K 2W
10K 10W
7.5K* 1W
SET UPPER
SET LOWER
7.5K* 1W
330
uF
33K
.01
V3
5
6
2
20K*
.01
1
7
.01
V4
100 mmF
100 mmF
.001
V5
470K
150*
470K
.01
47
.1
EXT
.01
INT
47K
10K 10W
½V6
7
200K*
.01
SET MAX.
100K*
100K HELIPOT
50K WW
LOWER DISC. BIAS
20K WW
100K
100 MA
10K*
M
E1
22K
75V
100 mmF
SET ZERO
V22
47K
SET ZERO
100K HELIPOT
20K WW
CHANNEL WIDTH
20K
3V
2.2K
22K
10K 10W
47K
UPPER DISC BIAS
.01
100K*
50K WW
.01
22K
SET
TOR

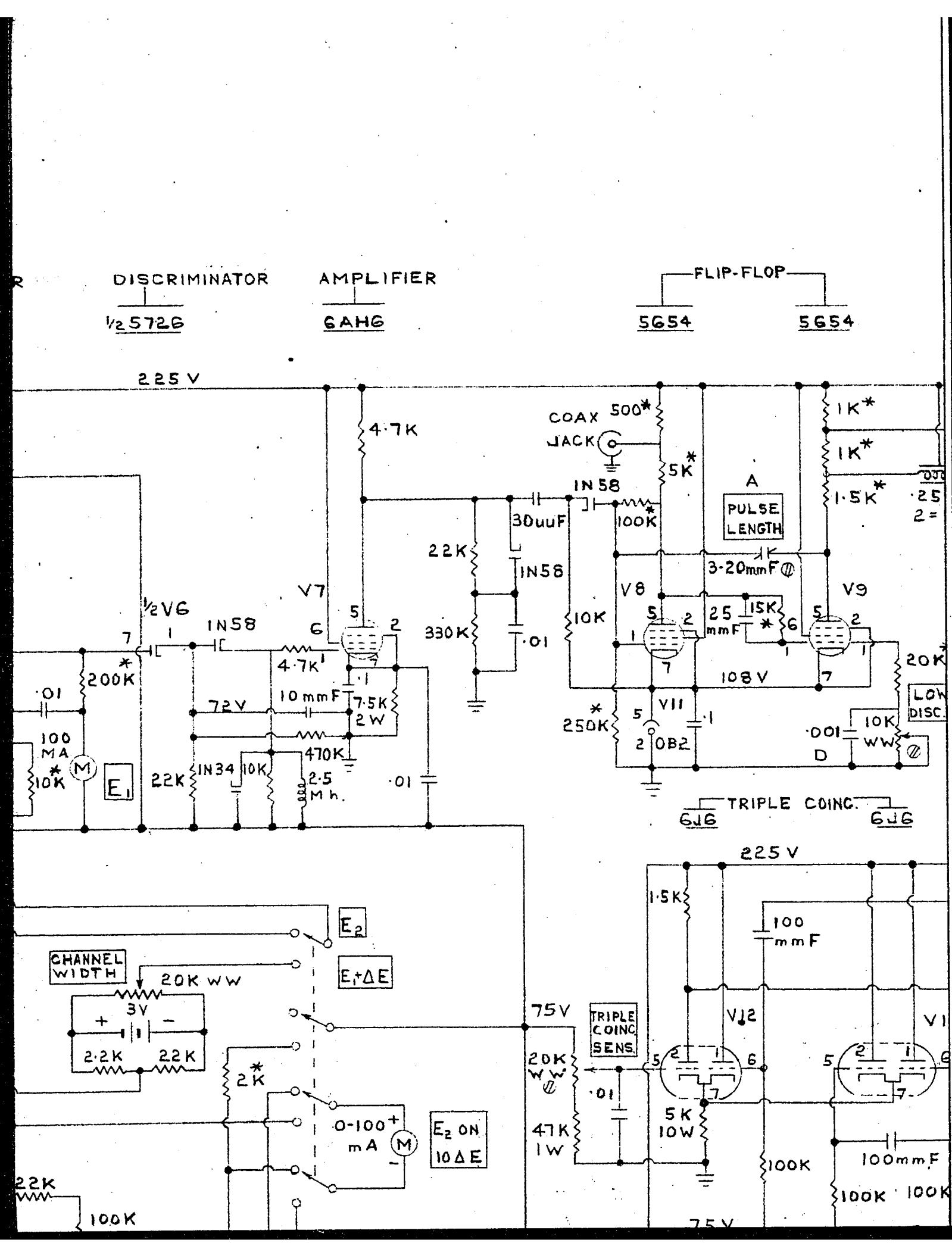
DISCRIMINATOR
AMPLIFIER
FLIP-FLOP
½ 5726
6AH6
5654
5654
225 V
4·7K
COAX JACK
500*
5K*
IN58
100K*
30uuF
22K
IN58
330K
·01
10K
A
PULSE LENGTH
3-20mmF
1K*
1K*
1·5K*
·25
2=
V7
V8
V9
½ V6
IN58
200K*
·01
100 MA
10K*
M
E1
72V
10 mmF
7·5K 2W
4·7K
470K
22K
IN34
10K
2·5 Mh.
·01
25 mmF
15K*
108 V
20K*
LOW DISC.
250K*
V11
0B2
·001
10K WW
D
TRIPLE COINC.
6J6
6J6
225 V
1·5K
100 mmF
E2
E1+ΔE
CHANNEL WIDTH
20K WW
3V
2·2K
22K
2K*
0-100 mA
M
E2 ON 10ΔE
75V
TRIPLE COINC SENS.
20K WW
·01
47K 1W
V12
V11
5K 10W
100K
100mmF
100K
100K
22K
100K
75V

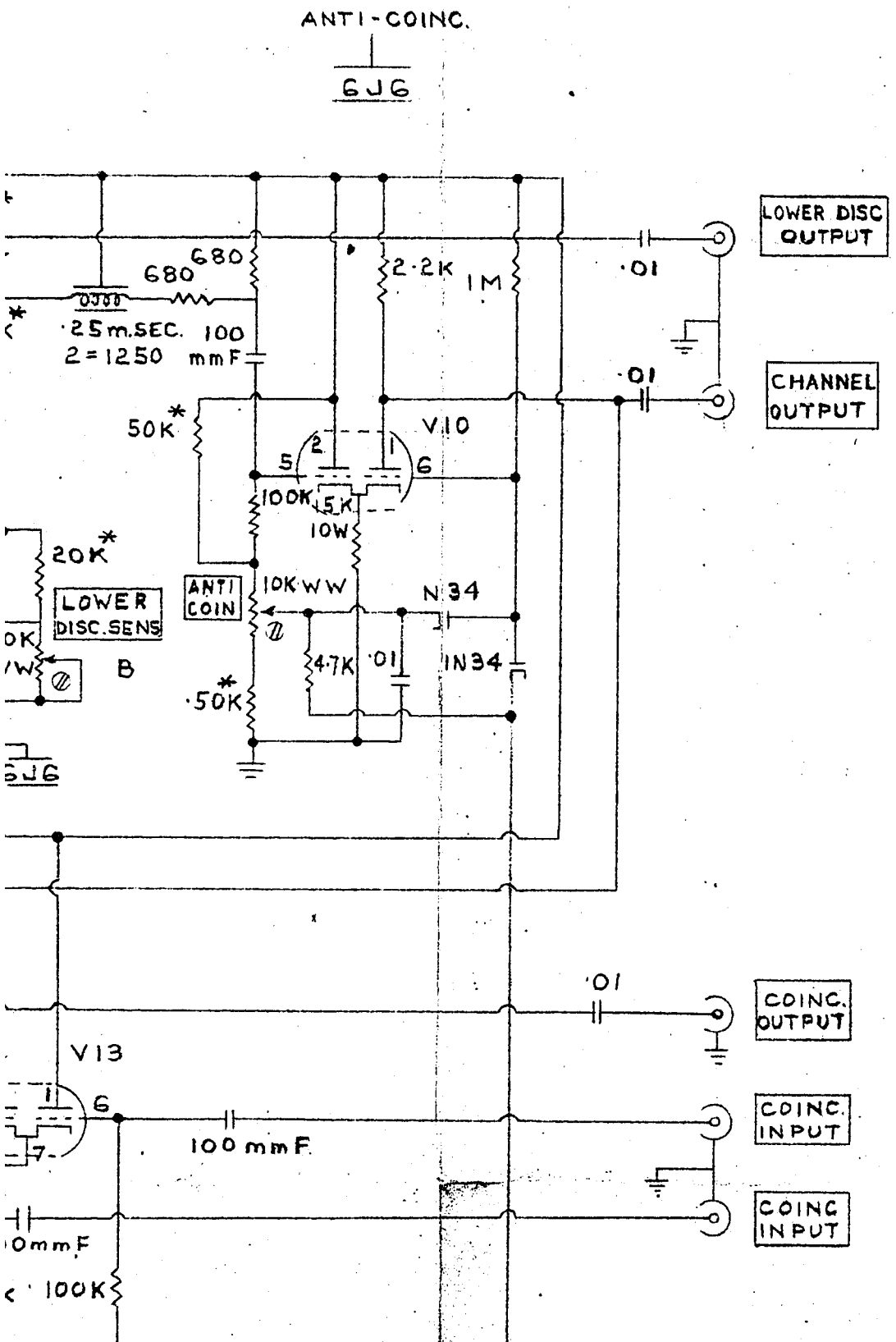
ANTI-COINC.
6J6
LOWER DISC OUTPUT
CHANNEL OUTPUT
COINC. OUTPUT
COINC. INPUT
COINC INPUT
680
680
2·2K
1M
·01
·25m.SEC.
2=1250
100 mmF
50K*
V10
100K
1.5K
10W
20K*
LOWER DISC.SENS
B
ANTI COIN
10K WW
N34
4·7K
·01
IN34
·50K*
6J6
V13
100 mmF.
100K

DET. NO.	

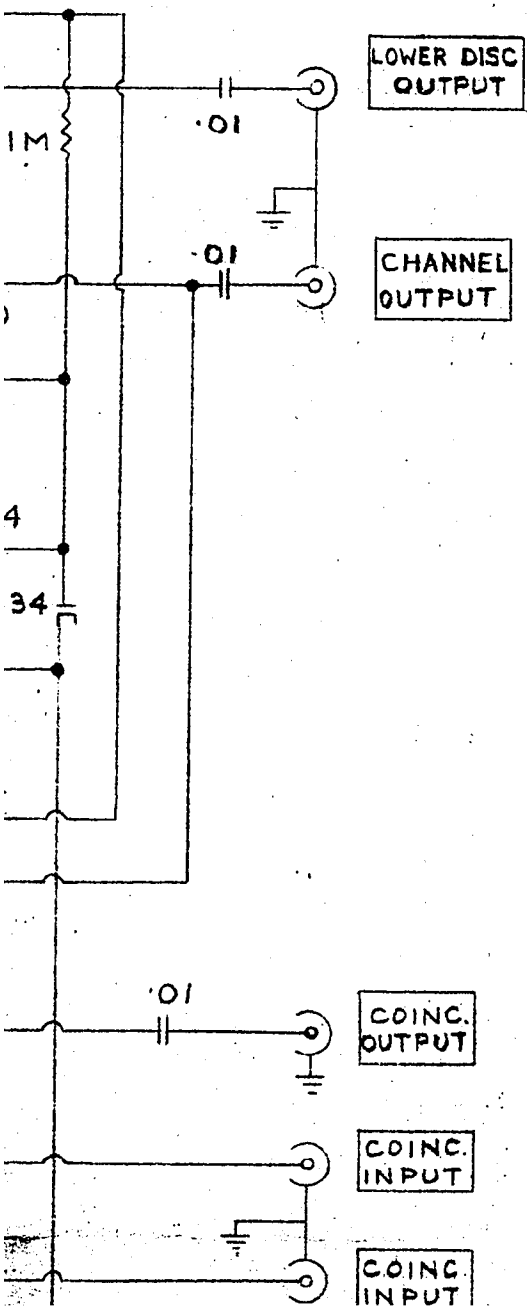

ORDER LIST

DET. NO.	DESCRIPTION	NO. REQ'D.

VOLTAGE REGUL

6080

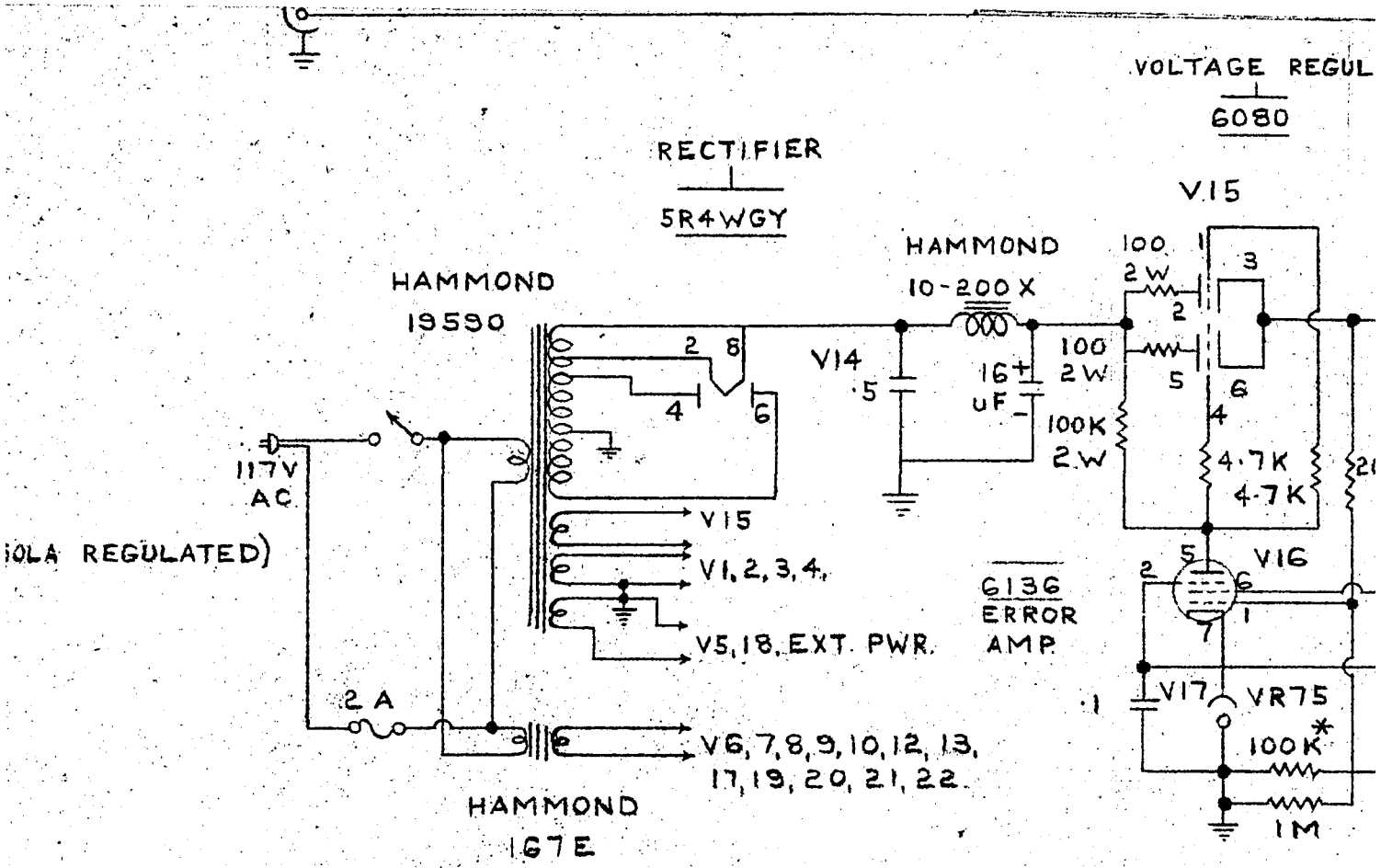

*- NOBLELOY 1% RESISTORS

Ø- SCREWDRIVER ADJUSTMENT.

A- ADJUST FOR 1 uSEC. PULSE.

B- ADJUST FOR 12V BIAS ON 5654 GRID.

C- ADJUST FOR CANCELLING AT ZERO CHANNEL

D- MAY BE 200 mmF ON SOME CHASSIS.

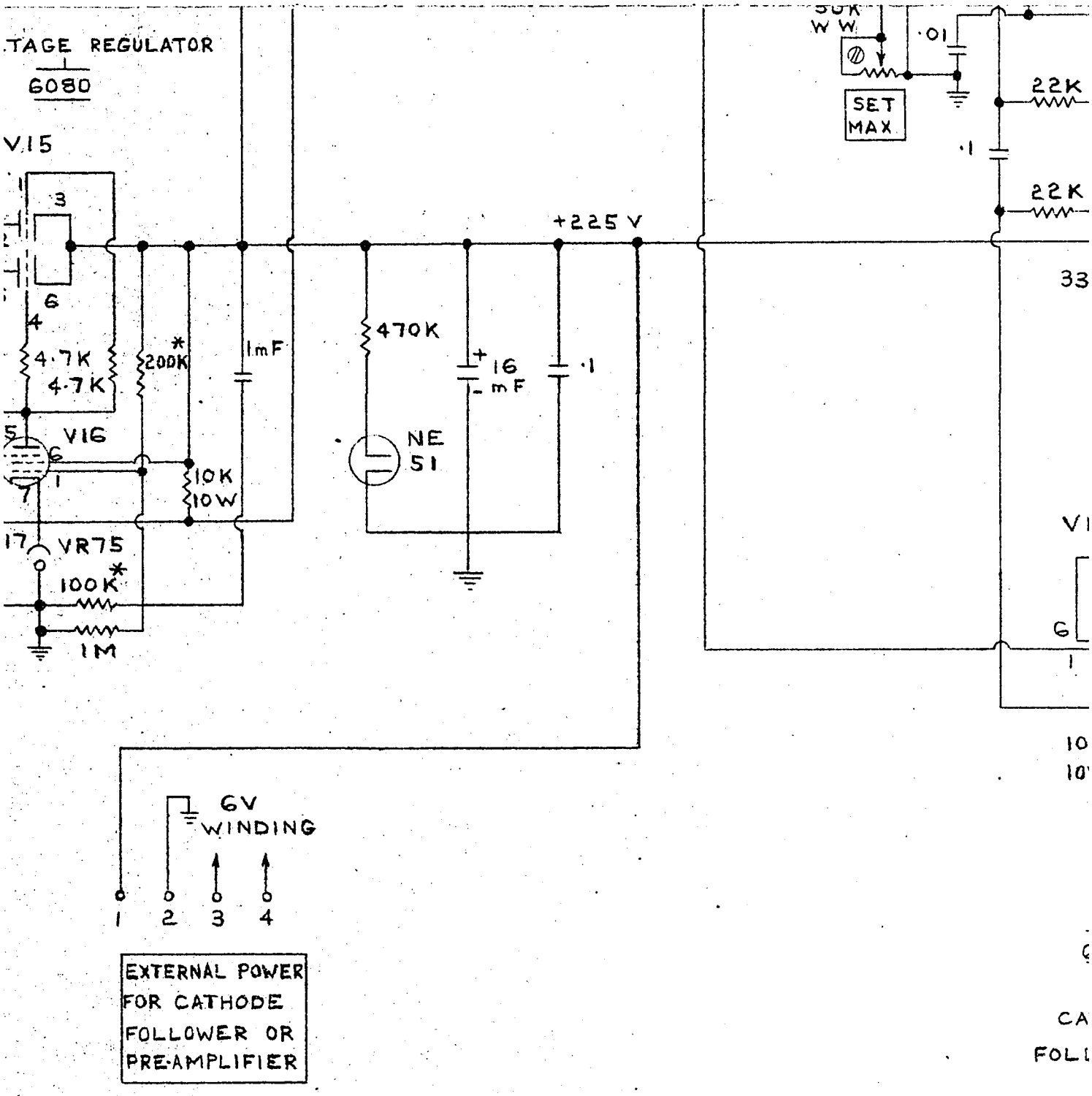
TAGE REGULATOR
6080
V15
3
6
4
4·7K
4·7K
*
200K
1mF
+225 V
470K
+
16
- mF
·1
NE
51
5
V16
6
1
7
10K
10W
17
VR75
100K*
1M
50K
W W
·01
SET
MAX
22K
·1
22K
33
6
1
6V
WINDING
1 2 3 4
EXTERNAL POWER
FOR CATHODE
FOLLOWER OR
PRE-AMPLIFIER

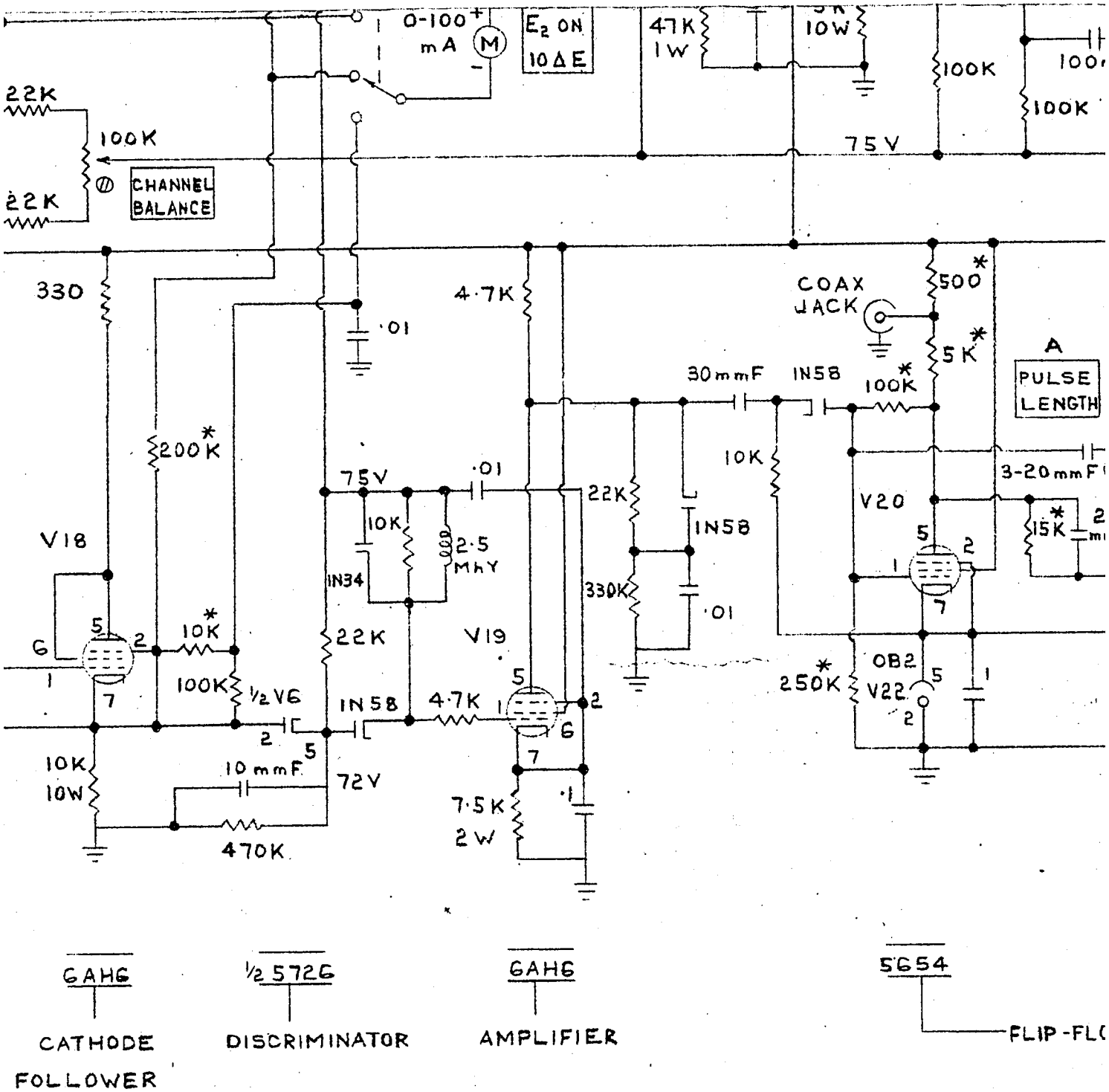
0-100 mA
M
E2 ON
10ΔE
47K 1W
10W
100K
100K
100K
75V
22K
100K
22K
CHANNEL BALANCE
330
200K*
.01
4.7K
COAX JACK
500*
5K*
A
PULSE LENGTH
30mmF
IN58
100K*
10K
3-20mmF
V20
15K*
75V
.01
22K
10K
2.5 MhY
IN34
IN58
330K
.01
V18
V19
10K*
22K
100K
½ V6
IN58
4.7K
10K 10W
10 mmF
72V
470K
7.5K 2W
.1
250K*
OB2
V22
6AH6
½ 5726
6AH6
5654
CATHODE FOLLOWER
DISCRIMINATOR
AMPLIFIER
FLIP-FL

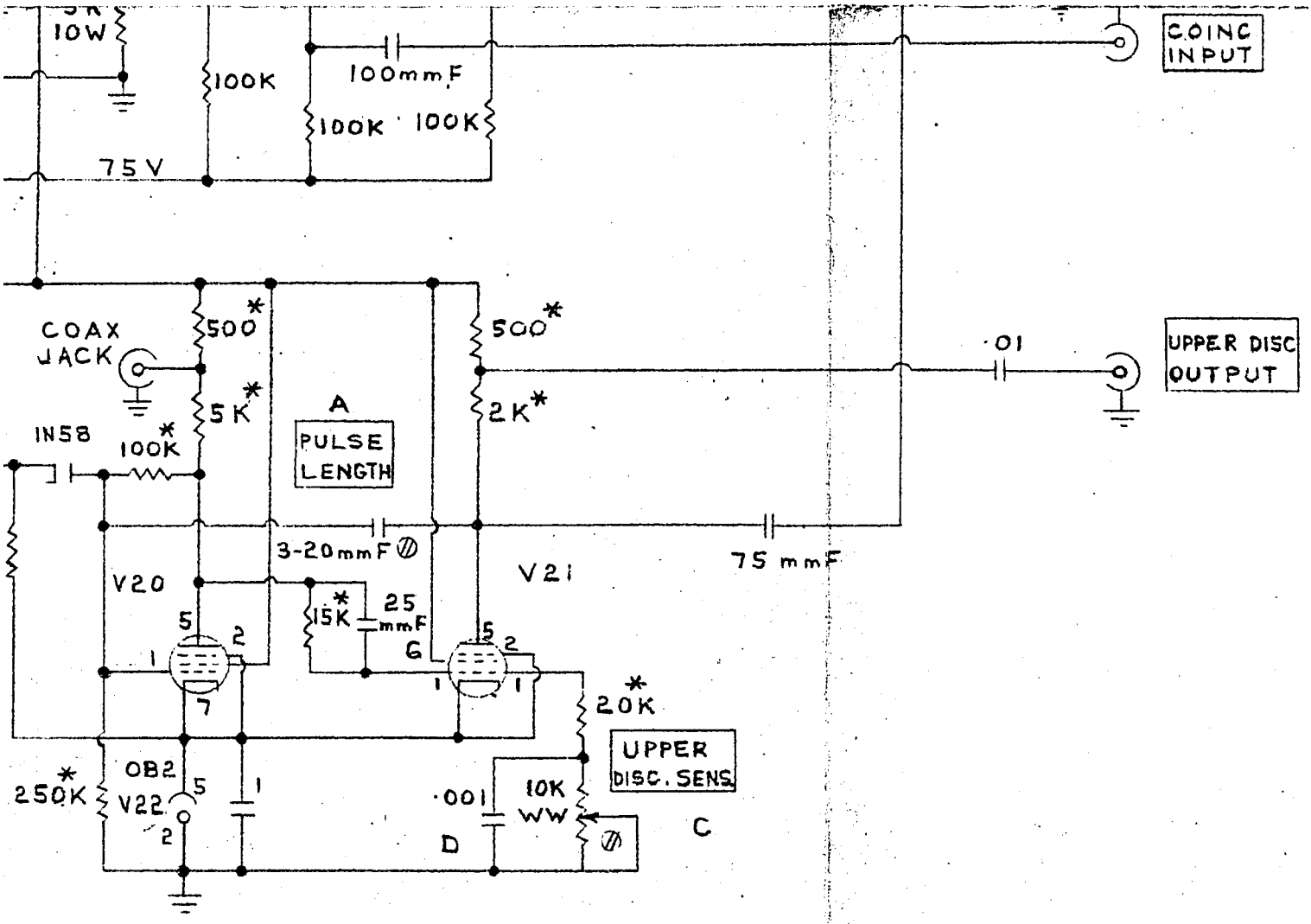

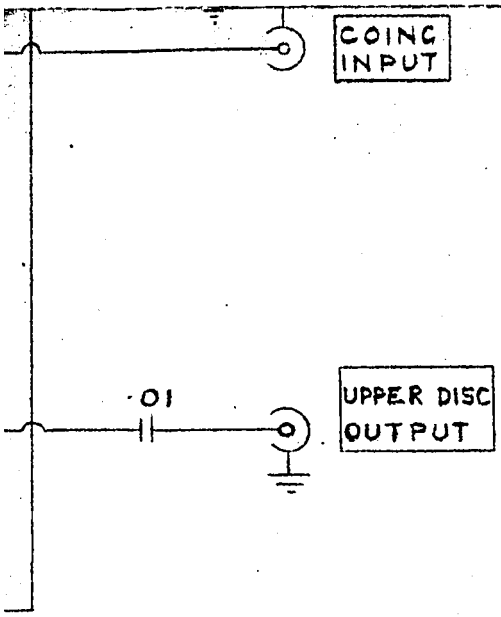

DATE	REVISIONS	BY	CHK'D	APP'D

REFERENCE DRAWINGS	DESCRIPTION

TOLERANCE ON ALL FRACTIONAL DIMENSIONS
PLUS MINUS UNLESS SHOWN OTHERWISE

FINISHED SURFACES

f1 ROUGH MACHINED
f2 ORDINARY MACHINED
f3 FINE MACHINED
f4 GROUND
f5 POLISHED

ALL FINISHED SURFACES TO BE f2 UNLESS OTHERWISE SHOWN.

FOR OFFICIAL USE ONLY

FOR OFFICIAL USE ONLY

JUL 5 1954

Print No. 46

WIRING DIAGRAM FOR PULSE HEIGHT ANALYZER

SCALE	DRAWN J. MORRIS	DATE 4/5/54
BLDG. NO. 233	CHECKED WHB	DATE Jul 27-54
JOB NO. 1934	APPROVED K. Lowrey	DATE July 27

ATOMIC ENERGY OF CANADA LIMITED
CHALK RIVER ONTARIO, CANADA

DE - 1934 - A

K. & E. CO., MONTREAL, 1951